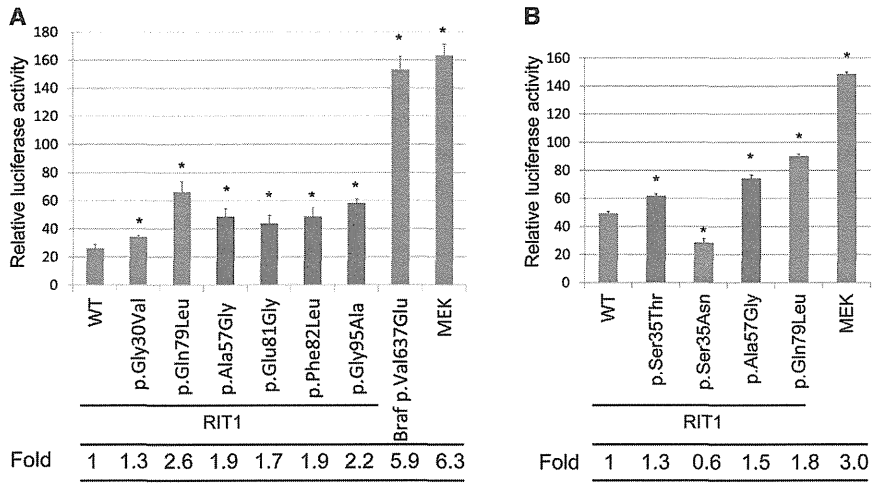

Figure 2. Stimulation of ELK Transcription in NIH 3T3 Cells Expressing *RIT1* Germline Mutations

(A) The ELK1-GAL4 vector and the GAL4 luciferase *trans*-reporter vector were transiently transfected with various *RIT1* germline mutations and activating mutations in *BRAF* and *MAP2K1* in NIH 3T3 cells. c.1910T>A (p.Val637Glu) in mouse *Braf* corresponds to oncogenic c.1799T>A (p.Val600Glu) in human *BRAF*. Relative luciferase activity was calculated by normalization to the activity of a cotransfected control vector, phRLnull-luc, containing distinguishable *R. reniformis* luciferase.

(B) ELK1 transactivation in cells expressing p.Ser35Thr, identified in individuals with Noonan syndrome, and p.Ser35Asn, were examined. p.Ser35Asn corresponds to dominant-negative alteration p.Ser17Asn in RAS.

Results are expressed as the means of quadruplicate (A) and triplicate (B) samples. Error bars represent the SDs of mean values. Red bars indicate germline *RIT1* mutations identified in Noonan syndrome. The following abbreviation is used: WT, wild-type. *$p < 0.01$ by t test.

abnormalities and were diagnosed with Noonan syndrome by diagnostic criteria developed by van der Burgt (Figures 1A–1L and Table 1).[4] Two individuals (NS358 and KCC38) were suspected to have CFC syndrome in the infantile period because of curly, sparse hair, a high cranial vault, and hypoplasia of the supraorbital ridges. Nine individuals showed perinatal abnormality, including polyhydramnios, nuchal translucency, and chylothorax (Table S2). It is of note that one individual (Og45) showing severe pleural effusion, hypertrophic cardiomyopathy, and hepatomegaly that ended in severe body edema and compromised circulation died 53 days after birth. Seven individuals showed high birth weight, probably as a result of subcutaneous edema, which is a typical manifestation observed in individuals with Noonan syndrome.[4] Out of 17 affected individuals, 16 (94%) had heart defects (Table 1): hypertrophic cardiomyopathy (HCM) in 12 (71%) individuals, pulmonary stenosis in 11 (65%) individuals, and atrial septal defects in 5 (29%) individuals. The incidence of pulmonic stenosis and mild cognitive defects is close to the overall incidence of these features in Noonan syndrome cohorts. By contrast, the incidence of HCM is far greater than in individuals with Noonan syndrome overall (25/118 in Noonan syndrome[42] versus 12/17 in individuals with *RIT1* mutations; $p < 0.0001$ by Fisher's exact test). It is of note that a high frequency of HCM (70%) was also reported in individuals with *RAF1* mutations.[10,11,24] It is possible that RIT1 interacts with RAF1 and that gain-of-function mutations in *RIT1* and *RAF1* exert similar effects in heart development.

Somatic alterations in classical RAS have been identified in approximately 30% of tumors.[43] Noonan syndrome and related disorders confer an increased risk of developing malignant tumors.[20,44] In a summary of the literature, it has been reported that 45 of 1,151 (3.9%) individuals with Noonan syndrome (but with an unknown mutation status) developed malignant tumors.[44] Since molecular analysis became available, gene-specific association with malignant tumors has been revealed. The association with JMML, a myeloproliferative disorder characterized by the excessive production of myelomonocytic cells, has been reported in individuals with *PTPN11*, *CBL*, and *KRAS* mutations. Recent reports showed that two individuals with *SOS1* mutations developed embryonal rhabdomyosarcoma.[45,46] A somatic *RIT1* variant, c.270G>A (p.Met90Ile), has been identified in lung cancer (COSMIC database). In the present cohort, 1 (NS168) of 17 individuals with *RIT1* c.242A>G (p.Glu81Gly) developed acute lymphoblastic leukemia at the age of 5 years. The child was treated by a standard protocol and has remained in complete remission. Examining whether gain-of-function mutations in *RIT1* cause tumorigenesis will require further study.

RIT1 has been isolated as a cDNA encoding highly conserved G3 and G4 domains of RAS proteins[33] or identified as a gene encoding a protein related to *Drosophila Ric*, a calmodulin-binding RAS-related GTPase.[34] RIT1 p.Gln79Leu, which corresponds to RAS p.Gln61Leu, is implicated in transforming NIH 3T3 cells, neurite outgrowth in neuronal cells, and the activation of ERK and p38 MAPK in a cell-specific manner.[37,38,47] In this study, enhanced ELK1 transactivation was observed in cells expressing mutant *RIT1* cDNAs. Previous studies showed that enhanced ELK transactivation was observed in NIH 3T3 cells expressing *HRAS*, *KRAS*, *BRAF*, and *RAF1* mutations identified in individuals with Costello, CFC, and Noonan syndromes.[17,18,24] Gastrulation defects observed in zebrafish embryos expressing RIT1 alterations (p.Glu81Gly, p.Gly95Ala, or p.Gln79Leu) were also reported in zebrafish embryos expressing an activating mutation in *NRAS*, *BRAF*, *MAP2K1*, or *MAP2K2*.[40,48] Taken together, these

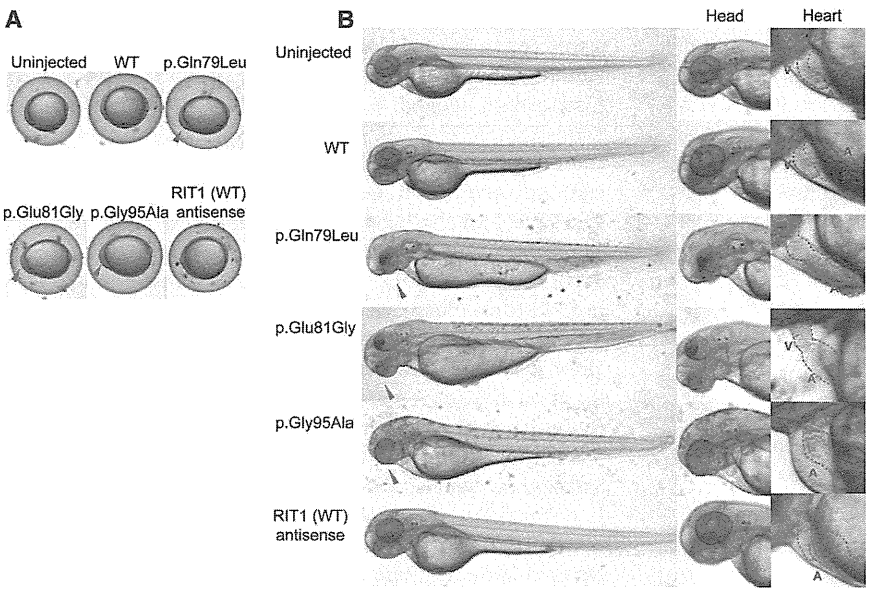

Figure 3. Morphology of Embryos Injected with the WT or Mutant *RIT1* mRNA

In vitro transcription of each mRNA was performed with the mMESSAGE mMACHINE kit (Applied Biosystems) according to the manufacturer's instructions. Synthesized mRNAs were purified with G-50 Micro Columns (GE Healthcare) and subsequently adjusted to a 300 ng/μl concentration for microinjection. Approximately 1 nl (300 pg) of RNA in water with 0.2% phenol red was injected into the cytoplasm of 1-cell-stage zebrafish embryos. Injected embryos were incubated at 28°C until observation.

(A) At 11 hpf, the shapes of the embryos injected with the WT sense or antisense mRNA were round, a normal morphology as observed in the uninjected embryos. In contrast, embryos expressing mutations (c.236A>T [p.Gln79Leu], c.242A>G [p.Glu81Gly], and c.284G>C [p.Gly95Ala]) are oval and compressed along the dorsal-ventral axis, indicative of a gastrulation defect. Note that cells have a hump in the head region at the anterior end of the body axis, the earliest manifestation of a craniofacial defect.

(B) Lateral views at 48 hpf are shown. Embryos expressing mutations (c.236A>T [p.Gln79Leu], c.242A>G [p.Glu81Gly], and c.284G>C [p.Gly95Ala]) formed swollen yolk sacs equally along the anterior posterior axis but did not show narrowing in the caudal half, which was clearly visible in the uninjected embryos and in those injected with the WT sense or antisense mRNA. In the craniofacial area, misshapen head and jaw structures and small eyes with hypoplasia on the ventral side were observed (middle panel); these phenotypes are consistent with the gastrulation defect. Shapes of the hearts (highlighted by red dotted lines) are shown in the right panel at a higher magnification. Normal looping of the heart tube and correct formation of two distinct chambers are observed in embryos injected with the WT sense or antisense mRNA. When mutations (c.236A>T [p.Gln79Leu], c.242A>G [p.Glu81Gly], and c.284G>C [p.Gly95Ala]) were expressed, looping was incomplete, resulting in stretched straight heart tubes. Constrictions at the atrial-ventricular canal are obscure, and the heart chambers are hypoplastic. Abbreviations are as follows: A, atrium; and V, ventricle.

results indicate that gain-of-function mutations in *RIT1* cause Noonan syndrome and show a similar effect to mutations in other RASopathy-related genes in human development.

Herein, we used whole-exome sequencing to identify germline *RIT1* mutations in individuals with Noonan syndrome, a disorder of the RASopathies. Mutations in *PTPN11*, *SOS1*, *RAF1*, *KRAS*, *BRAF*, and *NRAS* have been identified in 41%, 11%, 5%, 1%, 0.8%, and 0.2% of all cases, respectively,[3] and thus the frequency of *RIT1* mutations in Noonan syndrome might be similar to that of *RAF1* mutations. Our findings will improve diagnostic accuracy of Noonan syndrome and provide a clue to understanding the disorder's pathogenesis, including therapeutic approaches.

Supplemental Data

Supplemental Data include four figures, three tables, and six movies and can be found with this article online at http://www.cell.com/AJHG/.

Acknowledgments

The authors thank the families and the doctors who participated in this study. We are grateful to Jun-ichi Miyazaki at Osaka University for supplying the pCAGGS expression vector. We thank Yoko Narumi, Tomoko Kobayashi, Shoko Komatsuzaki, Yu Abe, Yuka Saito, Rumiko Izumi, Mitsuji Moriya, and Masako Yaoita for contributing to routine diagnostic work and Yoko Tateda, Kumi Kato, and Riyo Takahashi for their technical assistance. We are grateful to Eric Haan for sending samples of Noonan syndrome

Table 2. Morphologic Abnormality at 48–52 hpf of Zebrafish Embryos Injected with WT or Mutant RNA at the 1-Cell Stage

	No Abnormalities	Heart and Facial Abnormalities[a]	Severely Disorganized[b]	Total Number of Embryos
WT	125	7 (5.3%)	0 (0%)	132
p.Gln79Leu	31	78 (66.1%)	9 (7.6%)	118
p.Glu81Gly	42	55 (52.4%)	8 (7.6%)	105
p.Gly95Ala	44	34 (40.5%)	6 (7.1%)	84

[a]Craniofacial abnormalities, pericardial heart edema, and an elongated yolk sac were observed.
[b]Disorganized round body shape with a dysmorphic head and body trunk as shown in Figure S4.

and related disorders. We also acknowledge the support of the Biomedical Research Core of Tohoku University Graduate School of Medicine. This work was supported by the Funding Program for the Next Generation of World-Leading Researchers (NEXT Program) from the Ministry of Education, Culture, Sports, Science, and Technology of Japan (MEXT) to Y.A. (LS004), by Grants-in-Aids from MEXT, from the Japan Society for the Promotion of Science, and from the Ministry of Health, Labor, and Welfare to Y.M. and T.N. This work was supported in part by the National Cancer Center Research and Development Fund (23-22-11).

Received: April 23, 2013
Revised: May 19, 2013
Accepted: May 23, 2013
Published: June 20, 2013

Web Resources

The URLs for data presented herein are as follows:

Catalogue of Somatic Mutations in Cancer (COSMIC), http://www.sanger.ac.uk/genetics/CGP/cosmic/

Online Mendelian Inheritance in Man (OMIM), http://www.omim.org

RefSeq, http://www.ncbi.nlm.nih.gov/RefSeq

The RAS/MAPK Syndromes Homepage, http://www.medgen.med.tohoku.ac.jp/RasMapk%20syndromes.html

References

1. Takai, Y., Sasaki, T., and Matozaki, T. (2001). Small GTP-binding proteins. Physiol. Rev. *81*, 153–208.
2. Giehl, K. (2005). Oncogenic Ras in tumour progression and metastasis. Biol. Chem. *386*, 193–205.
3. Romano, A.A., Allanson, J.E., Dahlgren, J., Gelb, B.D., Hall, B., Pierpont, M.E., Roberts, A.E., Robinson, W., Takemoto, C.M., and Noonan, J.A. (2010). Noonan syndrome: clinical features, diagnosis, and management guidelines. Pediatrics *126*, 746–759.
4. van der Burgt, I. (2007). Noonan syndrome. Orphanet J. Rare Dis. *2*, 4.
5. Tartaglia, M., Mehler, E.L., Goldberg, R., Zampino, G., Brunner, H.G., Kremer, H., van der Burgt, I., Crosby, A.H., Ion, A., Jeffery, S., et al. (2001). Mutations in PTPN11, encoding the protein tyrosine phosphatase SHP-2, cause Noonan syndrome. Nat. Genet. *29*, 465–468.
6. Digilio, M.C., Conti, E., Sarkozy, A., Mingarelli, R., Dottorini, T., Marino, B., Pizzuti, A., and Dallapiccola, B. (2002). Grouping of multiple-lentigines/LEOPARD and Noonan syndromes on the PTPN11 gene. Am. J. Hum. Genet. *71*, 389–394.
7. Schubbert, S., Zenker, M., Rowe, S.L., Böll, S., Klein, C., Bollag, G., van der Burgt, I., Musante, L., Kalscheuer, V., Wehner, L.E., et al. (2006). Germline KRAS mutations cause Noonan syndrome. Nat. Genet. *38*, 331–336.
8. Roberts, A.E., Araki, T., Swanson, K.D., Montgomery, K.T., Schiripo, T.A., Joshi, V.A., Li, L., Yassin, Y., Tamburino, A.M., Neel, B.G., and Kucherlapati, R.S. (2007). Germline gain-of-function mutations in SOS1 cause Noonan syndrome. Nat. Genet. *39*, 70–74.
9. Tartaglia, M., Pennacchio, L.A., Zhao, C., Yadav, K.K., Fodale, V., Sarkozy, A., Pandit, B., Oishi, K., Martinelli, S., Schackwitz, W., et al. (2007). Gain-of-function SOS1 mutations cause a distinctive form of Noonan syndrome. Nat. Genet. *39*, 75–79.
10. Pandit, B., Sarkozy, A., Pennacchio, L.A., Carta, C., Oishi, K., Martinelli, S., Pogna, E.A., Schackwitz, W., Ustaszewska, A., Landstrom, A., et al. (2007). Gain-of-function RAF1 mutations cause Noonan and LEOPARD syndromes with hypertrophic cardiomyopathy. Nat. Genet. *39*, 1007–1012.
11. Razzaque, M.A., Nishizawa, T., Komoike, Y., Yagi, H., Furutani, M., Amo, R., Kamisago, M., Momma, K., Katayama, H., Nakagawa, M., et al. (2007). Germline gain-of-function mutations in RAF1 cause Noonan syndrome. Nat. Genet. *39*, 1013–1017.
12. Cirstea, I.C., Kutsche, K., Dvorsky, R., Gremer, L., Carta, C., Horn, D., Roberts, A.E., Lepri, F., Merbitz-Zahradnik, T., König, R., et al. (2010). A restricted spectrum of NRAS mutations causes Noonan syndrome. Nat. Genet. *42*, 27–29.
13. Cordeddu, V., Di Schiavi, E., Pennacchio, L.A., Ma'ayan, A., Sarkozy, A., Fodale, V., Cecchetti, S., Cardinale, A., Martin, J., Schackwitz, W., et al. (2009). Mutation of SHOC2 promotes aberrant protein N-myristoylation and causes Noonan-like syndrome with loose anagen hair. Nat. Genet. *41*, 1022–1026.
14. Loh, M.L., Sakai, D.S., Flotho, C., Kang, M., Fliegauf, M., Archambeault, S., Mullighan, C.G., Chen, L., Bergstraesser, E., Bueso-Ramos, C.E., et al. (2009). Mutations in CBL occur frequently in juvenile myelomonocytic leukemia. Blood *114*, 1859–1863.
15. Niemeyer, C.M., Kang, M.W., Shin, D.H., Furlan, I., Erlacher, M., Bunin, N.J., Bunda, S., Finklestein, J.Z., Sakamoto, K.M., Gorr, T.A., et al. (2010). Germline CBL mutations cause developmental abnormalities and predispose to juvenile myelomonocytic leukemia. Nat. Genet. *42*, 794–800.
16. Pérez, B., Mechinaud, F., Galambrun, C., Ben Romdhane, N., Isidor, B., Philip, N., Derain-Court, J., Cassinat, B., Lachenaud, J., Kaltenbach, S., et al. (2010). Germline mutations of the CBL gene define a new genetic syndrome with predisposition to juvenile myelomonocytic leukaemia. J. Med. Genet. *47*, 686–691.
17. Aoki, Y., Niihori, T., Kawame, H., Kurosawa, K., Ohashi, H., Tanaka, Y., Filocamo, M., Kato, K., Suzuki, Y., Kure, S., and Matsubara, Y. (2005). Germline mutations in HRAS proto-oncogene cause Costello syndrome. Nat. Genet. *37*, 1038–1040.
18. Niihori, T., Aoki, Y., Narumi, Y., Neri, G., Cavé, H., Verloes, A., Okamoto, N., Hennekam, R.C., Gillessen-Kaesbach, G., Wieczorek, D., et al. (2006). Germline KRAS and BRAF mutations in cardio-facio-cutaneous syndrome. Nat. Genet. *38*, 294–296.
19. Rodriguez-Viciana, P., Tetsu, O., Tidyman, W.E., Estep, A.L., Conger, B.A., Cruz, M.S., McCormick, F., and Rauen, K.A. (2006). Germline mutations in genes within the MAPK pathway cause cardio-facio-cutaneous syndrome. Science *311*, 1287–1290.
20. Aoki, Y., Niihori, T., Narumi, Y., Kure, S., and Matsubara, Y. (2008). The RAS/MAPK syndromes: novel roles of the RAS pathway in human genetic disorders. Hum. Mutat. *29*, 992–1006.
21. Tidyman, W.E., and Rauen, K.A. (2009). The RASopathies: developmental syndromes of Ras/MAPK pathway dysregulation. Curr. Opin. Genet. Dev. *19*, 230–236.
22. Groesser, L., Herschberger, E., Ruetten, A., Ruivenkamp, C., Lopriore, E., Zutt, M., Langmann, T., Singer, S., Klingseisen, L., Schneider-Brachert, W., et al. (2012). Postzygotic HRAS and KRAS mutations cause nevus sebaceous and Schimmelpenning syndrome. Nat. Genet. *44*, 783–787.

23. Abe, Y., Aoki, Y., Kuriyama, S., Kawame, H., Okamoto, N., Kurosawa, K., Ohashi, H., Mizuno, S., Ogata, T., Kure, S., et al.; Costello and CFC syndrome study group in Japan. (2012). Prevalence and clinical features of Costello syndrome and cardio-facio-cutaneous syndrome in Japan: findings from a nationwide epidemiological survey. Am. J. Med. Genet. A. *158A*, 1083–1094.
24. Kobayashi, T., Aoki, Y., Niihori, T., Cavé, H., Verloes, A., Okamoto, N., Kawame, H., Fujiwara, I., Takada, F., Ohata, T., et al. (2010). Molecular and clinical analysis of RAF1 in Noonan syndrome and related disorders: dephosphorylation of serine 259 as the essential mechanism for mutant activation. Hum. Mutat. *31*, 284–294.
25. Komatsuzaki, S., Aoki, Y., Niihori, T., Okamoto, N., Hennekam, R.C., Hopman, S., Ohashi, H., Mizuno, S., Watanabe, Y., Kamasaki, H., et al. (2010). Mutation analysis of the SHOC2 gene in Noonan-like syndrome and in hematologic malignancies. J. Hum. Genet. *55*, 801–809.
26. Narumi, Y., Aoki, Y., Niihori, T., Neri, G., Cavé, H., Verloes, A., Nava, C., Kavamura, M.I., Okamoto, N., Kurosawa, K., et al. (2007). Molecular and clinical characterization of cardio-facio-cutaneous (CFC) syndrome: overlapping clinical manifestations with Costello syndrome. Am. J. Med. Genet. A. *143A*, 799–807.
27. Narumi, Y., Aoki, Y., Niihori, T., Sakurai, M., Cavé, H., Verloes, A., Nishio, K., Ohashi, H., Kurosawa, K., Okamoto, N., et al. (2008). Clinical manifestations in patients with SOS1 mutations range from Noonan syndrome to CFC syndrome. J. Hum. Genet. *53*, 834–841.
28. Niihori, T., Aoki, Y., Okamoto, N., Kurosawa, K., Ohashi, H., Mizuno, S., Kawame, H., Inazawa, J., Ohura, T., Arai, H., et al. (2011). HRAS mutants identified in Costello syndrome patients can induce cellular senescence: possible implications for the pathogenesis of Costello syndrome. J. Hum. Genet. *56*, 707–715.
29. Saito, Y., Aoki, Y., Muramatsu, H., Makishima, H., Maciejewski, J.P., Imaizumi, M., Rikiishi, T., Sasahara, Y., Kure, S., Niihori, T., et al. (2012). Casitas B-cell lymphoma mutation in childhood T-cell acute lymphoblastic leukemia. Leuk. Res. *36*, 1009–1015.
30. Li, H., and Durbin, R. (2009). Fast and accurate short read alignment with Burrows-Wheeler transform. Bioinformatics *25*, 1754–1760.
31. McKenna, A., Hanna, M., Banks, E., Sivachenko, A., Cibulskis, K., Kernytsky, A., Garimella, K., Altshuler, D., Gabriel, S., Daly, M., and DePristo, M.A. (2010). The Genome Analysis Toolkit: a MapReduce framework for analyzing next-generation DNA sequencing data. Genome Res. *20*, 1297–1303.
32. Wang, K., Li, M., and Hakonarson, H. (2010). ANNOVAR: functional annotation of genetic variants from high-throughput sequencing data. Nucleic Acids Res. *38*, e164.
33. Lee, C.H., Della, N.G., Chew, C.E., and Zack, D.J. (1996). Rin, a neuron-specific and calmodulin-binding small G-protein, and Rit define a novel subfamily of ras proteins. J. Neurosci. *16*, 6784–6794.
34. Wes, P.D., Yu, M., and Montell, C. (1996). RIC, a calmodulin-binding Ras-like GTPase. EMBO J. *15*, 5839–5848.
35. van der Burgt, I., Kupsky, W., Stassou, S., Nadroo, A., Barroso, C., Diem, A., Kratz, C.P., Dvorsky, R., Ahmadian, M.R., and Zenker, M. (2007). Myopathy caused by HRAS germline mutations: implications for disturbed myogenic differentiation in the presence of constitutive HRas activation. J. Med. Genet. *44*, 459–462.
36. Niwa, H., Yamamura, K., and Miyazaki, J. (1991). Efficient selection for high-expression transfectants with a novel eukaryotic vector. Gene *108*, 193–199.
37. Rusyn, E.V., Reynolds, E.R., Shao, H., Grana, T.M., Chan, T.O., Andres, D.A., and Cox, A.D. (2000). Rit, a non-lipid-modified Ras-related protein, transforms NIH3T3 cells without activating the ERK, JNK, p38 MAPK or PI3K/Akt pathways. Oncogene *19*, 4685–4694.
38. Shi, G.X., and Andres, D.A. (2005). Rit contributes to nerve growth factor-induced neuronal differentiation via activation of B-Raf-extracellular signal-regulated kinase and p38 mitogen-activated protein kinase cascades. Mol. Cell. Biol. *25*, 830–846.
39. Cai, W., Rudolph, J.L., Harrison, S.M., Jin, L., Frantz, A.L., Harrison, D.A., and Andres, D.A. (2011). An evolutionarily conserved Rit GTPase-p38 MAPK signaling pathway mediates oxidative stress resistance. Mol. Biol. Cell *22*, 3231–3241.
40. Runtuwene, V., van Eekelen, M., Overvoorde, J., Rehmann, H., Yntema, H.G., Nillesen, W.M., van Haeringen, A., van der Burgt, I., Burgering, B., and den Hertog, J. (2011). Noonan syndrome gain-of-function mutations in NRAS cause zebrafish gastrulation defects. Dis Model Mech *4*, 393–399.
41. Fürthauer, M., Van Celst, J., Thisse, C., and Thisse, B. (2004). Fgf signalling controls the dorsoventral patterning of the zebrafish embryo. Development *131*, 2853–2864.
42. Burch, M., Sharland, M., Shinebourne, E., Smith, G., Patton, M., and McKenna, W. (1993). Cardiologic abnormalities in Noonan syndrome: phenotypic diagnosis and echocardiographic assessment of 118 patients. J. Am. Coll. Cardiol. *22*, 1189–1192.
43. Schubbert, S., Shannon, K., and Bollag, G. (2007). Hyperactive Ras in developmental disorders and cancer. Nat. Rev. Cancer *7*, 295–308.
44. Kratz, C.P., Rapisuwon, S., Reed, H., Hasle, H., and Rosenberg, P.S. (2011). Cancer in Noonan, Costello, cardiofaciocutaneous and LEOPARD syndromes. Am. J. Med. Genet. C. Semin. Med. Genet. *157*, 83–89.
45. Denayer, E., Devriendt, K., de Ravel, T., Van Buggenhout, G., Smeets, E., Francois, I., Sznajer, Y., Craen, M., Leventopoulos, G., Mutesa, L., et al. (2010). Tumor spectrum in children with Noonan syndrome and SOS1 or RAF1 mutations. Genes Chromosomes Cancer *49*, 242–252.
46. Jongmans, M.C.J., Hoogerbrugge, P.M., Hilkens, L., Flucke, U., van der Burgt, I., Noordam, K., Ruiterkamp-Versteeg, M., Yntema, H.G., Nillesen, W.M., Ligtenberg, M.J.L., et al. (2010). Noonan syndrome, the SOS1 gene and embryonal rhabdomyosarcoma. Genes Chromosomes Cancer *49*, 635–641.
47. Hynds, D.L., Spencer, M.L., Andres, D.A., and Snow, D.M. (2003). Rit promotes MEK-independent neurite branching in human neuroblastoma cells. J. Cell Sci. *116*, 1925–1935.
48. Anastasaki, C., Estep, A.L., Marais, R., Rauen, K.A., and Patton, E.E. (2009). Kinase-activating and kinase-impaired cardio-facio-cutaneous syndrome alleles have activity during zebrafish development and are sensitive to small molecule inhibitors. Hum. Mol. Genet. *18*, 2543–2554.

Journal of Human Genetics (2013) 58, 259–266

www.nature.com/jhg

ORIGINAL ARTICLE

Exome sequencing identifies a novel *TTN* mutation in a family with hereditary myopathy with early respiratory failure

Rumiko Izumi[1,2], Tetsuya Niihori[1], Yoko Aoki[1], Naoki Suzuki[2], Masaaki Kato[2], Hitoshi Warita[2], Toshiaki Takahashi[3], Maki Tateyama[2], Takeshi Nagashima[4], Ryo Funayama[4], Koji Abe[5], Keiko Nakayama[4], Masashi Aoki[2] and Yoichi Matsubara[1]

Myofibrillar myopathy (MFM) is a group of chronic muscular disorders that show the focal dissolution of myofibrils and accumulation of degradation products. The major genetic basis of MFMs is unknown. In 1993, our group reported a Japanese family with dominantly inherited cytoplasmic body myopathy, which is now included in MFM, characterized by late-onset chronic progressive distal muscle weakness and early respiratory failure. In this study, we performed linkage analysis and exome sequencing on these patients and identified a novel c.90263G>T mutation in the *TTN* gene (NM_001256850). During the course of our study, another groups reported three mutations in *TTN* in patients with hereditary myopathy with early respiratory failure (HMERF, MIM #603689), which is characterized by overlapping pathologic findings with MFMs. Our patients were clinically compatible with HMERF. The mutation identified in this study and the three mutations in patients with HMERF were located on the A-band domain of titin, suggesting a strong relationship between mutations in the A-band domain of titin and HMERF. Mutation screening of *TTN* has been rarely carried out because of its huge size, consisting of 363 exons. It is possible that focused analysis of *TTN* may detect more mutations in patients with MFMs, especially in those with early respiratory failure.
Journal of Human Genetics (2013) **58,** 259–266; doi:10.1038/jhg.2013.9; published online 28 February 2013

Keywords: A-band; cytoplasmic body; Fn3 domain; hereditary myopathy with early respiratory failure; HMERF; myofibrillar myopathy; titin; *TTN*

INTRODUCTION

Myofibrillar myopathies (MFMs) were proposed in 1996 as a group of chronic muscular disorders characterized by common morphologic features observed on muscle histology, which showed the focal dissolution of myofibrils followed by the accumulation of products of the degradative process.[1] The clinical phenotype of MFM is characterized by slowly progressive muscle weakness that can involve proximal or distal muscles, with onset in adulthood in most cases. However, other phenotypes are highly variable. Although 20% of patients with MFMs have been revealed to have mutations in *DES*, *CRYAB*, *MYOT*, *LDB* (*ZASP*), *FLNC* or *BAG3*, the major genetic basis of MFMs remains to be elucidated.

Respiratory weakness is one of the symptoms of MFMs. The early or initial presentation of respiratory failure is not a common manifestation of MFMs as a whole, and there are limited reports regarding a fraction of patients with *DES*,[2] *MYOT*[3] or *CRYAB*[4] mutation. In 1993, our group reported a Japanese family with dominantly inherited cytoplasmic body (CB) myopathy,[5] which is now included in MFM. Currently, this family includes 20 patients in five successive generations who show almost homogeneous clinical features characterized by chronic progressive distal muscle weakness and early respiratory failure. However, the underlying genetic etiology in this family was unknown. The aim of this study was to determine the genetic cause in this family. To identify the responsible genetic mutation, we performed linkage analysis and whole-exome sequencing.

MATERIALS AND METHODS

This study was approved by the Ethics Committee of the Tohoku University School of Medicine, and all individuals gave their informed consent before their inclusion in the study.

[1]Department of Medical Genetics, Tohoku University School of Medicine, Sendai, Japan; [2]Department of Neurology, Tohoku University School of Medicine, Sendai, Japan; [3]Department of Neurology and Division of Clinical Research, National Hospital Organization Nishitaga National Hospital, Sendai, Japan; [4]Division of Cell Proliferation, United Centers for Advanced Research and Translational Medicine, Tohoku University Graduate School of Medicine, Sendai, Japan and [5]Department of Neurology, Okayama University Medical School, Okayama, Japan
Correspondence: Dr Y Aoki, Department of Medical Genetics, Tohoku University School of Medicine, 1-1 Seiryo-machi, Aoba-ku, Sendai 980-8574, Japan.
E-mail: aokiy@med.tohoku.ac.jp
or Professor M Aoki, Department of Neurology, Tohoku University School of Medicine, 1-1 Seiryo-machi, Aoba-ku, Sendai 980-8574, Japan.
E-mail: aokim@med.tohoku.ac.jp
Received 23 October 2012; revised 9 January 2013; accepted 10 January 2013; published online 28 February 2013

Clinical information on the family

This family includes 20 patients (13 males and 7 females) in five successive generations (Figure 1). The family is of Japanese ancestry, and no consanguineous or international mating was found. Of all patients, seven underwent a muscle biopsy, and two were autopsied. All of the histological findings were compatible with MFM (see clinical data).

The age of onset ranged from 27–45 years. The most common presenting symptom was foot drop. At the initial evaluations, muscle weakness was primarily distributed in the ankle dorsiflexors and finger extensors. The patients were generally built and showed no other extramuscular abnormalities. In addition to this chronic progressive distal muscle weakness, respiratory distress occurred between 0 and 7 years from the initial onset (average 3.8 years) in seven patients (IV-9, V-2, A, B, E, H, and J) with adequate clinical information. Two patients who had not had any respiratory care died of respiratory failure approximately a decade from the initial onset. The other patients have been alive for more than 10 years (maximum 18 years) but require nocturnal non-invasive positive pressure ventilation. They were 37–58 years of age as of 2012 and able to walk independently with or without a simple walking aid. Although the time at which patients recognized dysphagia or dysarthria varied between 1 to more than 10 years from the initial onset, decreased bulbar functions had been noted at the initial evaluation in most cases. Cardiac function was normally maintained in all patients of the family.

Clinical data

The level of serum creatine kinase was normal or mildly elevated. Electromyography of affected muscles showed a chronic myogenic pattern, and the nerve conduction study did not suggest any neuropathic involvement. Muscle imaging showed focal atrophy in the tibialis anterior, tibialis posterior, extensor hallucis and digitorum longus, peroneal and semitendinosus muscle on initial assessment (Figure 2A), and atrophy became clear in cervical muscles, shoulder girdles, intercostals and proximal limb muscles in the following several years. Upon muscle biopsy, the most common finding was numerous cytoplasmic bodies (CBs), which were found on 7.3% of myofibers in the tibialis anterior of individual E (Figure 2B (a–c)) and 50–80% of intercostals in other cases.[5] Other nonspecific findings were increased variability in the size of myofibers, central nuclei and rimmed vacuoles observed on a few fibers. No strong immunoreaction of desmin was seen in the CBs (Figure 2B (d, e)). An electron microscope examination showed that the regular sarcoplasmic pattern was replaced by abnormal fine filamentous structures, which seemed to attach to the Z-band. CBs were also found in almost all skeletal muscles and some smooth muscles in autopsied cases.[5] Cardiac myofibers also contained numerous CBs in one of the autopsied cases (V-2),[5] although the patient did not present any cardiac complication. The sequence analysis of the coding regions and flanking introns of *DES* and *MYOT* showed no pathogenic mutation in individual E. An array comparative genomic hybridization performed with the Agilent SurePrint G3 Human CGH 1M microarray format in individual A did not reveal any aberrations of genomic copy number.

Linkage analysis

DNA was extracted by standard methods. Linkage analysis was performed on nine family members (A–I in Figure 1; four of them were affected, and the others were unaffected) through genotyping using an Illumina Human Omni 2.5 BeadChip (Illumina, San Diego, CA, USA). We chose single-nucleotide polymorphisms (SNPs) that satisfied all of the following criteria: (1) autosomal SNPs whose allele frequencies were available from the HapMap project (http://hapmap.ncbi.nlm.nih.gov/), (2) SNPs that were not monomorphic among members and (3) SNPs that were not in strong linkage disequilibrium with neighboring SNPs (r2 values <0.9). Then, we selected the first five SNPs from each position of integer genetic distance from SNPs that met the above criteria for the initial analysis. The details were as follows; we chose a SNP closest to 0 cM and the neighboring four SNPs. If the genetic distance of a SNP was the same as that of the next SNP, we considered the genomic position to determine their order. We repeated this process at 1 cM, 2 cM and so on.

We performed a multipoint linkage analysis of the data set (17 613 SNPs) using MERLIN[6] 1.1.2 under the autosomal dominant mode with the following parameters: 0.0001 for disease allele frequency, 1.00 for individuals heterozygous and homozygous for the disease allele and 0.00 for individuals

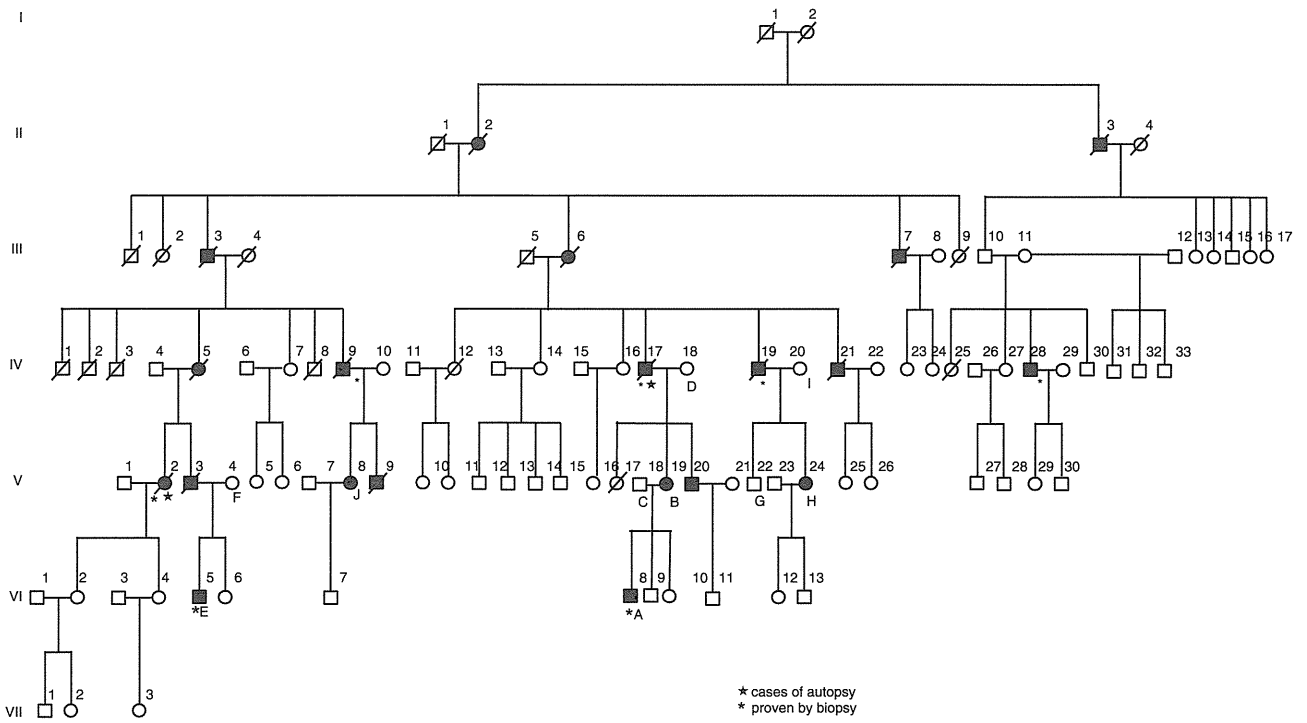

Figure 1 Family pedigree. Filled-in symbols indicate individuals with MFM. Empty symbols indicate unaffected individuals. A star and asterisk indicate autopsy-proven and muscle biopsy-proven cases, respectively. (A–J) indicates individuals whose DNA was used for this study.

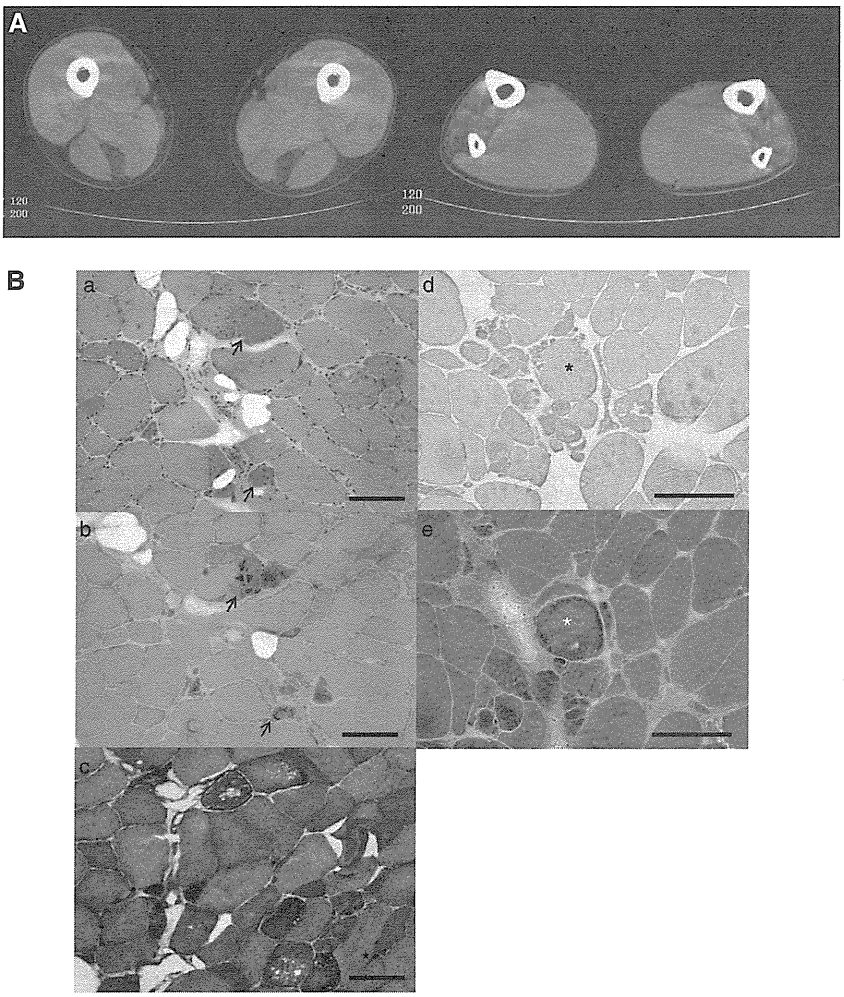

Figure 2 Family clinical data. (**A**) Muscle computed tomography of affected lower extremity. The imaging in the initial assessment of individual A showed symmetrical atrophy and fatty replacement of the semitendinosus in the proximal lower extremities (left) and the tibialis anterior, tibialis posterior, extensor hallucis and digitorum longus, and peroneal muscle in the distal (right) lower extremities. (**B**) Pathology of muscle biopsy. Hematoxylin-eosin (a), Gomori-trichrome (b) and NADH (nicotinamide adenine dinucleotide)-tetrazolium reductase (c) staining of the muscle biopsy sample from the tibialis anterior of individual E are shown. CBs are indicated by arrows. CBs were round or oval, 5–10 μm in diameter and predominantly located in the periphery of type 1 fibers, which stained eosinophilic with hematoxylin-eosin and blue–purple with Gomori-trichrome. NADH-tetrazolium reductase staining showed disorganization of the myofibrillar network. Immunostaining for desmin (d) and Gomori-trichrome staining (e) are serial sections of the muscle biopsy from individual E. Stars indicate corresponding fibers. No strong immunoreaction of desmin was seen in the CBs. Scale bars = 100 μm

homozygous for the alternative allele. After this first analysis, a second analysis was performed with all SNPs fulfilling the above criteria around the peaks identified in the first analysis.

Exome sequencing

Exome sequencing was performed on seven family members in three generations (A–E, H and I in Figure 1), four of whom were affected. Exon capture was performed with the SureSelect Human All Exon kit v2 (individuals E, H and I) or v4 (A–D) (Agilent Technologies, Santa Clara, CA, USA). Exon libraries were sequenced with the Illumina Hiseq 2000 platform according to the manufacturer's instructions (Illumina). Paired 101-base pair reads were aligned to the reference human genome (UCSChg19) using the Burrows-Wheeler Alignment tool.[7] Likely PCR duplicates were removed with the Picard program (http://picard.sourceforge.net/). Single-nucleotide variants and indels were identified using the Genome Analysis Tool Kit (GATK) v1.5 software.[8] SNVs and indels were annotated against the RefSeq database and dbSNP135 with the ANNOVAR program.[9] We used the PolyPhen2 polymorphism phenotyping software tool[10] to predict the functional effects of mutations.

Sanger sequencing

To confirm that mutations identified by exome sequencing segregated with the disease, we performed direct sequencing. PCR was performed with the primers shown in Supplementary Table 1. PCR products were purified with a MultiScreen PCR plate (Millipore, Billerica, MA, USA) and sequenced using BigDye terminator v1.1 and a 3500xL genetic analyzer (Applied Biosystems, Carlsbad, CA, USA).

RESULTS

Linkage analysis

The first linkage analysis identified five regions across autosomes with a logarithm of odds (LOD) score greater than 2 (Figure 3). Of the five regions, two were on chromosome 2 (from 167 cM to 168 cM, with a maximum LOD score of 2.46 and from 182 cM to 185 cM, with a maximum LOD score of 2.71), the other two were on chromosome 8 (from 27 cM to 34 cM, with a maximum LOD score of 2.71 and at 61 cM, with a maximum LOD score of 2.03), and one was on

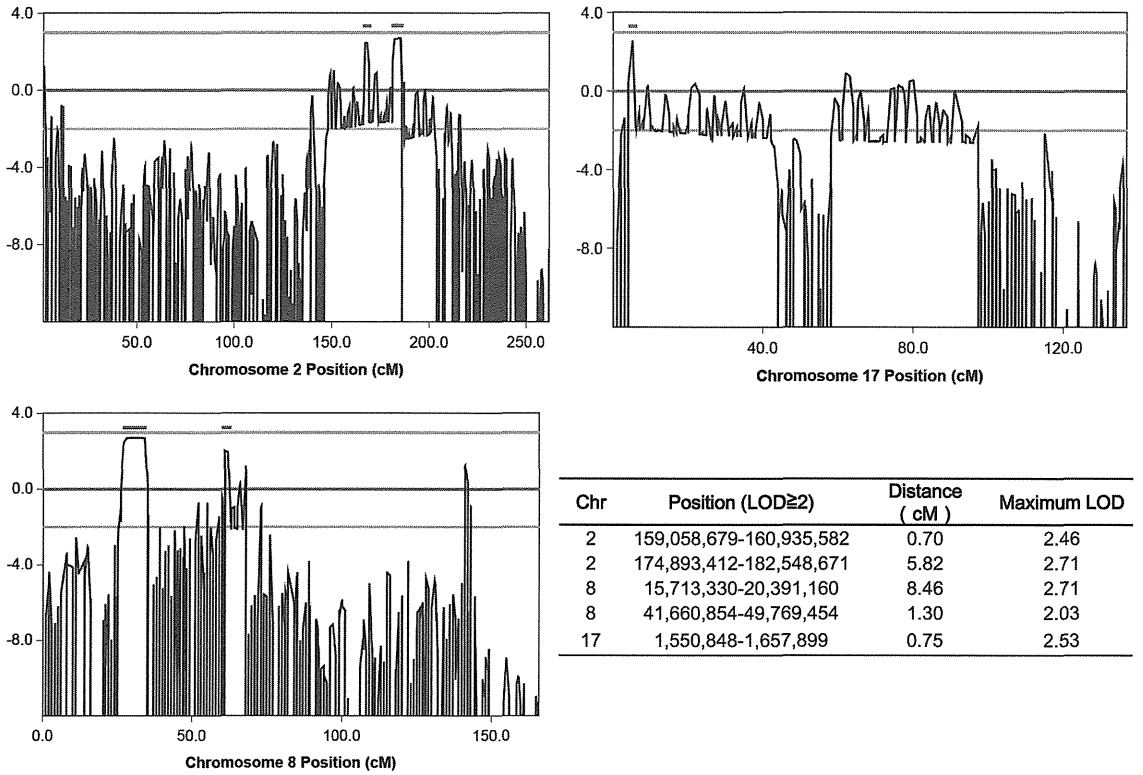

Chr	Position (LOD≥2)	Distance (cM)	Maximum LOD
2	159,058,679-160,935,582	0.70	2.46
2	174,893,412-182,548,671	5.82	2.71
8	15,713,330-20,391,160	8.46	2.71
8	41,660,854-49,769,454	1.30	2.03
17	1,550,848-1,657,899	0.75	2.53

Figure 3 Linkage analysis. Linkage analysis was performed on nine family members (four of them were affected, the others were unaffected) using an Illumina Human Omni 2.5 BeadChip. Five regions with an LOD score greater than 2 (indicated by bar) were identified. A full color version of this figure is available at the *Journal of Human Genetics* journal online.

Table 1 Summary of detected variants by exome sequencing

Individual *Morbidity*	*A* *Affected*	*B* *Affected*	*C* *Unaffected*	*D* *Unaffected*	*E* *Affected*	*H* *Affected*	*I* *Unaffected*	*Segregated in seven family members*
Exonic, splicing	10089	10064	10079	10065	10230	10194	10216	64
Nonsynonymous, splicing, indel, nonsense	4987	5020	5055	5038	5143	5234	5200	32
Allele frequency not available	577	600	536	555	671	794	786	2

chromosome 17 (at 5 cM, with a maximum LOD score of 2.53). In the second detailed linkage analysis, these peaks were determined to range from 167.49 cM at rs4233674 at position 159 058 679 to 168.19 cM at rs7598162 at position 160 935 582, and from 181.23 cM at rs4402725 at position 174 893 412 to 187.05 cM at rs7420169 at position 182 548 671 on chromosome 2; from 26.42 cM at rs2736043 at position 15 713 330 to 34.88 cM at rs9325871 at position 20 391 160, and from 61.02 cM at rs6999814 at position 41 660 854 to 62.32 cM at rs10957281 at position 49 769 454 on chromosome 8; and from 4.7 cM at rs11078552 at position 1 550 848 to 5.45 cM at rs1057355 at position 1 657 899 on chromosome 17. Haplotypes shared by affected individuals in these regions were confirmed by visual inspection. There were a few incompatible SNPs in these regions, presumably due to genotyping error.

Exome sequencing and segregation analysis

In exome sequencing, an average of 215 million reads enriched by SureSelect v4 (SSv4) and 319 million reads enriched by SureSelect v2 (SSv2) were generated, and 99% of reads were mapped to the reference genome by Burrows-Wheeler Alignment tool. An average of 57% (SSv4) and 61% (SSv2) of those reads were duplicated and removed, and an average of 80% (SSv4) and 66% (SSv2) of mapped reads without duplicates were in target regions. The average coverage of each exome was 163-fold (SSv4) and 130-fold (SSv2). An average of 85% (SSv4) and 69% (SSv2) of target regions were covered at least 50-fold (Supplementary Table 2). On average, 10 133 SNVs or indels, which are located within coding exons or splice sites, were identified per individual (Table 1). A total of 64 variants were common among patients and not present in unaffected individuals, and 32 of those were left after excluding synonymous SNVs. In these variants, only the heterozygous mutation c.90263G>T (NM_001256850) at position 179 410 777 of chromosome 2, which was predicted to p.W30088L in *TTN*, was novel (that is, not present in dbSNP v135 or 1000 genomes). Polyphen2 predicted this mutation as probably damaging. This mutation was located in a candidate region suggested by the linkage analysis in the present study. The other variants were registered with dbSNP135, and the allele frequencies, except for one SNV, rs138183879, in *IKBKB*, ranged from 0.0023 to 0.62.

a

Gene	Chr	Position	Variant type	Reference	Variant	dbSNP v135	Coding change	Prediction	Segregaion analysis
TTN	2	179 410777	Missense	G	T	Not present	W30088L	Probably damaging	Segregating
IKBKB	8	42 188 457	Missense	C	T	rs138183879	T742M	Benign	Non-segregating

b

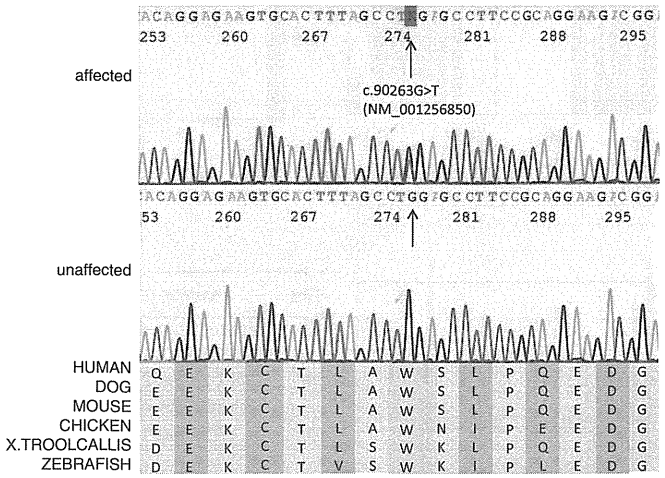

Figure 4 Identified mutations by exome sequencing. (**a**) We performed segregation analysis of two candidates. (**b**) The identified *TTN* mutation and its conservation among species. Sanger sequencing confirmed the heterozygous G to T substitution (indicated by the arrow) at the position chr2;179 410 777, which corresponds to c.90263G>T in exon 293 (NM_001256850.1). The substitution leads to p.W30088L (NP_001243779.1), and this amino acid is conserved among species.

These values were not compatible with the assumption that MFM was a rare disease and showed complete penetrance in this family. The allele frequency of rs138183879 was not available in dbSNP135, and this SNV was in the candidate region on chromosome 8 based on linkage analysis.

We then performed a segregation analysis on the two candidates, the novel mutation c.90263G>T in *TTN* and rs138183879 in *IKBKB*, through Sanger sequencing in 10 family members (A–J in Figure 1; Figure 4a). The rs138183879 SNP was not found in individual J, that is, it was not segregated with the disease in this family. In contrast, the novel mutation c.90263G>T in *TTN* was detected in all patients ($n=5$) and not detected in any of the unaffected family members ($n=5$) or 191 ethnically matched control subjects (382 chromosomes). These results suggested that this rare mutation in *TTN* segregated with the disease in this family.

DISCUSSION

In this study, we found that a novel missense mutation in *TTN* segregated with MFM in a large Japanese family. The identified c.90263G>T mutation in *TTN* (NM_001256850) was considered to be the genetic cause of MFM in our family, because (1) exome sequencing revealed that this was the best candidate mutation after filtering SNPs and indels, (2) this mutation is located in a region on chromosome 2 shared by affected family members, (3) the segregation with MFM was confirmed by Sanger sequencing, (4) this mutation was not detected in 191 control individuals, (5) this mutation was predicted to alter highly conserved amino acids (Figure 4b) and (6) *TTN* encodes a Z-disc-binding molecule called titin, which is similar to all of the previously identified causative genes for MFMs, which also encode Z-disc-associated molecules.

Recently, three mutations in *TTN* have been reported as the causes of hereditary myopathy with early respiratory failure (HMERF, MIM #603689),[11–16] which has similar muscle pathology to MFMs. The identified novel missense mutation c.90263G>T in our study was located on the same exon as recently reported HMERF mutations: c.90272C>T in a Portuguese family[16] and c.90315T>C in Swedish and English families[14,15] (Table 2). This finding suggests the possibility that our family can be recognized as having HMERF from a clinical aspect.

Compared with symptoms described in the past three reports on HMERF (also see Table 2), our patients have common features, such as autosomal dominant inheritance, early respiratory failure, the absence of clinically apparent cardiomyopathy, normal to mild elevation of serum CK and histological findings compatible with MFM. Early involvement of the tibialis anterior is also common, except for the Portuguese family, who reported isolated respiratory insufficiency and a milder presentation of HMERF. Thus, our family shares major clinical manifestations with patients with HMERF, suggesting that the identified mutation is novel for MFM and HMERF.

To date, mutations in *TTN* have been identified in skeletal myopathy and cardiomyopathy.[17,18] The relationship between the variant positions on *TTN* and phenotypes accompanied by skeletal or respiratory muscle involvement is summarized in Table 2. Titin is a large protein (4.20 MDa) that extends from the Z-disk to the M-line within the sarcomere, and it is composed of four major domains: Z-disc, I-band, A-band and M-line (Figure 5). All four HMERF mutations detected by other groups and our study were consistently located in the A-band domain, while mutations in tibial muscular dystrophy (TMD) (MIM #600334),[19–24] limb-girdle muscular dystrophy type 2J (LGMD2J) (#608807)[19,25] and early-onset myopathy with fatal cardiomyopathy (#611705)[26] were located in the M-line domain. HMERF and TMD have some common clinical characteristics, such as autosomal dominant inheritance with onset in adulthood and strong involvement of the tibialis anterior muscle.

Table 2 Previously reported TTN mutations with skeletal and/or respiratory muscle involvement

Phenotype	*LGMD*	*HMERF*	*Our family*	*HMERF*	*HMERF*	*TMD*	*TMD*	*LGMD2J*	*TMD*	*TMD*	*TMD*	*TMD*	*TMD*	*Early-onset myopathy with fatal cardiomyopathy*	*Early-onset myopathy with fatal cardiomyopathy*
Reported by	Vasli *et al.*[16]	Ohlsson *et al.*,[14] Pfeffer *et al.*[15]	Abe *et al.*[5]	Vasli *et al.*[16]	Edstrom *et al.*,[12] Nicolao, *et al.*[11] Lang e *et al.*[13]	Hackman *et al.*[23]	Udd *et al.*,[20] Hackman *et al.*[19]	Udd *et al.*,[25] Hackman *et al.*[19]	Pollazzon *et al.*[24]	Van den Bergh *et al.*[22]	Seze *et al.*,[21] Hackman *et al.*[19]	Hackman *et al.*[23]	Hackman *et al.*[23]	Carmignac *et al.*[26]	Carmignac *et al.*[26]
Mutation identified in Nucleotide (NM_001256850.1)	2012 c.3100G>A, c.52024G>A	2012 c.90315T>C	2012 c.90263G>T	2012 c.90272C>T	2005 c.97348C>T	2008 c.102724delT	2002 102857_102867 del11ins11	2002 102857_102867 del11ins11	2010 c.102914A>C	2003 c.102917T>A	2002 c.102944T>C	2008 c.102966delA	2008 c.102967C>T	2007 g.289385del ACCAAGTG	2007 g.291297delA
Protein (NP_001243779.1)	p.V1034M, p.A17342T	p.C30071R	p.W30088L	p.P30091L	p.R32450W				p.H34305P	p.I34306N	p.L34315P		p.Q34323X		
Domain	I-band, A-band	A-band (Fn3)	A-band (Fn3)	A-band (Fn3)	A-band (kinase)	M-line	M-line	M-line	M-line	M-line	M-line	M-line	M-line	M-line	M-line
Population	French	Swedish English	Japanese	Portuguese	Swedish	French	Finnish	Finnish	Italian	Belgian	French	Spanish	French	Sudanese	Moroccan
Inheritance	AR	AD	AD	AD	AD	AD	AD	AR	AD	AD	AD	AD	AD	Consanguineous siblings	Consanguineous siblings
Onset	35	33–71	27–45	46	20–50s	20–30s	35–55	20–30s	50–60s	47	45	40–50s	30s	Neonatal	Infant-early childhood
Skeletal muscles															
Major	Proximal UL and LL	TA, PL, EDL, ST	TA, ST	No	TA, neck flexor, proximals	TA, GA,HAM, pelvic	TA	All proximals	TA	TA	TA	TA	TA, HAM, pelvic	General muscle weakness and hypotonia	Psoas, TA, GA, peroneus
Minor		Neck flexor	Cervical, shoulder girdles, intercostals, proximal limb			QF				EDL, peroneal, TP	GA, femoral, scapular	HAM, GA	GA, distal UL		QF, proximal UL, neck, facial, trunk flexor
Spared			Facial			Proximal UL	Facial, UL, proximals	Facial		UL, proximal LL	Facial	UL	Proximal UL, QF		
Cardiac muscles	ND	No	No	ND	ND	ND	No	No	ND	ND	ND	ND	ND	DCM, onset; in the first decade	DCM, onset; 5–12 years old
Respiratory failure	ND	Yes, within 5–8 years	Yes, within 7 years	Isolated respiratory failure	Yes, as first presentation	ND	ND	ND	ND	ND	ND	ND	ND	ND	ND
Muscle pathologic features	ND	Inclusion bodies (major) and RVs (minor)	Cytoplasmic bodies (major) and RVs (minor)	Cytoplasmic bodies	Cytoplasmic bodies, positive for rhodamine-conjugated *phalloidin*	Dystrophic pattern without vacuoles	Nonspecific dystrophic change	Nonspecific dystrophic change, loss of calpain-3	Dystrophic pattern with RVs	Nonspecific, RV	Nonspecific	Dystrophic pattern with RVs	Nonspecific	Minicore-like lesions and abundant central nuclei	Minicore-like lesions and abundant central nuclei

Abbreviations: AD, autosomal dominant; AR, autosomal recessive; DCM, dilated cardiomyopathy; EDL, extensor digitorum longus; GA, gastrocnemius; HAM, hamstrings; LL, lower limb; ND, not described; no, no involvement; PL, peroneus longus; QF, quadriceps femoris; RV, rimmed vacuole;
ST, semitendinosus; TA, tibialis anterior; TMD, tibial muscular dystrophy; TP, tibialis posterior; UL, upper limb.

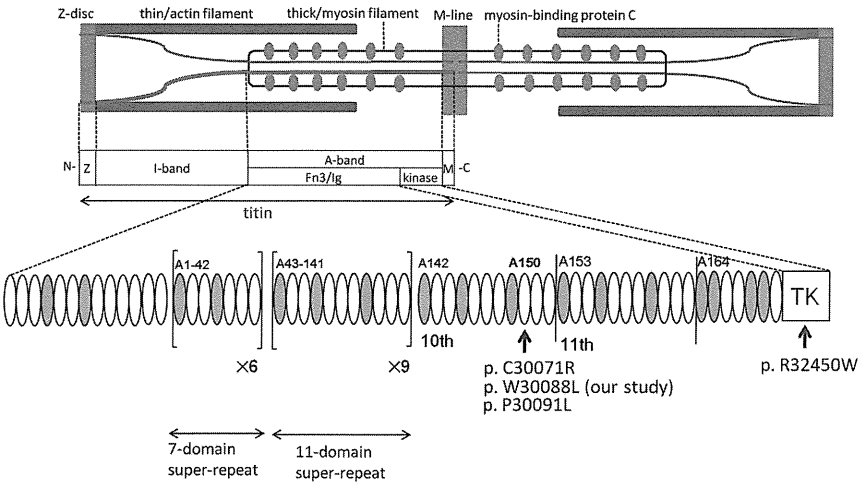

Figure 5 Structure of titin and mutation distribution in the A-band domain. Human *TTN* was mapped to 2q31.2. *TTN* is 294 kb and is composed of 363 exons that code for a maximum of 38 138 amino-acid residues and a 4.20-MDa protein[32] called titin. Titin is expressed in the cardiac and skeletal muscles and spans half the sarcomere, with its N-terminal at the Z-disc and the C-terminal at the M-line.[33] Titin is composed of four major domains: Z-disc, I-band, A-band and M-line. I-band regions of titin are thought to make elastic connections between the thick filament (that is, myosin filament) and the Z-disc within the sarcomere, whereas the A-band domain of titin seems to be bound to the thick filament, where it may regulate filament length and assembly.[34] The gray and white ellipses indicate an Ig-like domain and fibronectin type 3 domain, respectively. Our mutation (p.W30088L) and the neighboring two mutations (that is, p.C30071R and p.P30091L) were all located in the 6th Fn3 domain in the 10th domain of large super-repeats. A full color version of this figure is available at the *Journal of Human Genetics* journal online.

In contrast, one of the distinctive features of TMD is that early respiratory failure has not been observed in patients with TMD. Histological findings of TMD usually do not include CBs but show nonspecific dystrophic change. The underlying pathogenic processes explaining why mutations on these neighboring domains share some similarities but also some differences are unknown.

Three of four HMERF mutations in the A-band domain are located in the fibronectin type 3 and Ig-like (Fn3/Ig) domain, and one of four HMERF mutations is located in the kinase domain (Table 2, also see Figure 5). The missense mutation c.97348C>T in the kinase domain was the first reported HMERF mutation. It has been shown that the kinase domain has an important role in controlling muscle gene expression and protein turnover via the neighbor of BRCA1 gene-1-muscle-specific RING finger protein-serum response transcription factor pathway.[13] Moreover, the Fn3/Ig domain is composed of two types of super-repeats: six consecutive copies of 7-domain super-repeat at the N-terminus and 11 consecutive copies of 11-domain super-repeat at the C-terminus.[27–29] These super-repeats are highly conserved among species and muscles. Our identified mutation (c.90263G>T) and the neighboring two mutations (that is, c.90272C>T and c.90315T>C shown in Table 2) were all located on the 6th Fn3 domain in the 10th copy of 11-domain super-repeat (that is, A150 domain[30]) (Figure 5). Although some Fn3 domains are proposed to be the putative binding site for myosin,[31] the role with the majority of Fn3 domains, how it supports the structure of each repeat architecture, and the identity of its binding partner have not been fully elucidated. Our findings suggested that the Fn3 domain, in which mutations clustered, has critical roles in the pathogenesis of HMERF, although detailed mechanisms of pathogenesis remain unknown.

In conclusion, we have identified a novel disease-causing mutation in *TTN* in a family with MFM that was clinically compatible with HMERF. Because of its large size, global mutation screening of *TTN* has been difficult. Mutations in *TTN* may be detected by massively parallel sequencing in more patients with MFMs, especially in patients with early respiratory failure. Further studies are needed to understand the genotype–phenotype correlations in patients with mutations in *TTN* and the molecular function of titin.

ACKNOWLEDGEMENTS

We thank the patients and their family. We are grateful to Yoko Tateda, Kumi Kato, Naoko Shimakura, Risa Ando, Riyo Takahashi, Miyuki Tsuda, Nozomi Koshita, Mami Kikuchi and Kiyotaka Kuroda for their technical assistance. We also acknowledge the support of the Biomedical Research Core of Tohoku University Graduate School of Medicine. This work was supported by a grant of Research on Applying Health Technology provided by the Ministry of Health, Labor and Welfare to YM, an Intramural Research Grant (23-5) for Neurological and Psychiatric Disorders of NCNP and JSPS KAKENHI Grant number 24659421.

1 Nakano, S., Engel, A. G., Waclawik, A. J., Emslie-Smith, A. M. & Busis, N. A. Myofibrillar myopathy with abnormal foci of desmin positivity. I. Light and electron microscopy analysis of 10 cases. *J. Neuropathol. Exp. Neurol.* **55,** 549–562 (1996).
2 Olive, M., Odgerel, Z., Martinez, A., Poza, J. J., Bragado, F. G., Zabalza, R. J. *et al.* Clinical and myopathological evaluation of early- and late-onset subtypes of myofibrillar myopathy. *Neuromuscul. Disord.* **21,** 533–542 (2011).
3 Olive, M., Goldfarb, L. G., Shatunov, A., Fischer, D. & Ferrer, I. Myotilinopathy: refining the clinical and myopathological phenotype. *Brain* **128,** 2315–2326 (2005).
4 Selcen, D. & Engel, A. G. Myofibrillar myopathy caused by novel dominant negative alpha B-crystallin mutations. *Ann. Neurol.* **54,** 804–810 (2003).
5 Abe, K., Kobayashi, K., Chida, K., Kimura, N. & Kogure, K. Dominantly inherited cytoplasmic body myopathy in a Japanese kindred. *Tohoku. J. Exp. Med.* **170,** 261–272 (1993).
6 Abecasis, G. R., Cherny, S. S., Cookson, W. O. & Cardon, L. R. Merlin–rapid analysis of dense genetic maps using sparse gene flow trees. *Nat. Genet.* **30,** 97–101 (2002).
7 Li, H. & Durbin, R. Fast and accurate short read alignment with Burrows-Wheeler transform. *Bioinformatics* **25,** 1754–1760 (2009).
8 McKenna, A., Hanna, M., Banks, E., Sivachenko, A., Cibulskis, K., Kernytsky, A. *et al.* The Genome Analysis Toolkit: a MapReduce framework for analyzing next-generation DNA sequencing data. *Genome. Res.* **20,** 1297–1303 (2010).
9 Wang, K., Li, M. & Hakonarson, H. ANNOVAR: functional annotation of genetic variants from high-throughput sequencing data.. *Nucleic Acids Res.* **38,** e164 (2010).
10 Adzhubei, I. A., Schmidt, S., Peshkin, L., Ramensky, V. E., Gerasimova, A., Bork, P. *et al.* A method and server for predicting damaging missense mutations. *Nat. Methods* **7,** 248–249 (2010).
11 Nicolao, P., Xiang, F., Gunnarsson, L. G., Giometto, B., Edstrom, L., Anvret, M. *et al.* Autosomal dominant myopathy with proximal weakness and early respiratory muscle involvement maps to chromosome 2q. *Am. J. Hum. Genet.* **64,** 788–792 (1999).

12 Edstrom, L., Thornell, L. E., Albo, J., Landin, S. & Samuelsson, M. Myopathy with respiratory failure and typical myofibrillar lesions. *J. Neurol. Sci.* **96,** 211–228 (1990).
13 Lange, S., Xiang, F., Yakovenko, A., Vihola, A., Hackman, P., Rostkova, E. *et al.* The kinase domain of titin controls muscle gene expression and protein turnover. *Science* **308,** 1599–1603 (2005).
14 Ohlsson, M., Hedberg, C., Bradvik, B., Lindberg, C., Tajsharghi, H., Danielsson, O. *et al.* Hereditary myopathy with early respiratory failure associated with a mutation in A-band titin. *Brain* **135,** 1682–1694 (2012).
15 Pfeffer, G., Elliott, H. R., Griffin, H., Barresi, R., Miller, J., Marsh, J. *et al.* Titin mutation segregates with hereditary myopathy with early respiratory failure. *Brain* **135,** 1695–1713 (2012).
16 Vasli, N., Bohm, J., Le Gras, S., Muller, J., Pizot, C., Jost, B. *et al.* Next generation sequencing for molecular diagnosis of neuromuscular diseases. *Acta. Neuropathol.* **124,** 273–283 (2012).
17 Kontrogianni-Konstantopoulos, A., Ackermann, M. A., Bowman, A. L., Yap, S. V. & Bloch, R. J. Muscle giants: molecular scaffolds in sarcomerogenesis. *Physiol. Rev.* **89,** 1217–1267 (2009).
18 Ottenheijm, C. A. & Granzier, H. Role of titin in skeletal muscle function and disease. *Adv. Exp. Med. Biol.* **682,** 105–122 (2010).
19 Hackman, P., Vihola, A., Haravuori, H., Marchand, S., Sarparanta, J., De Seze, J. *et al.* Tibial muscular dystrophy is a titinopathy caused by mutations in TTN, the gene encoding the giant skeletal-muscle protein titin. *Am. J. Hum. Genet.* **71,** 492–500 (2002).
20 Udd, B., Partanen, J., Halonen, P., Falck, B., Hakamies, L., Heikkila, H. *et al.* Tibial muscular dystrophy. Late adult-onset distal myopathy in 66 Finnish patients. *Arch. Neurol.* **50,** 604–608 (1993).
21 de Seze, J., Udd, B., Haravuori, H., Sablonniere, B., Maurage, C. A., Hurtevent, J. F. *et al.* The first European family with tibial muscular dystrophy outside the Finnish population. *Neurology* **51,** 1746–1748 (1998).
22 Van den Bergh, P. Y., Bouquiaux, O., Verellen, C., Marchand, S., Richard, I., Hackman, P. *et al.* Tibial muscular dystrophy in a Belgian family. *Ann. Neurol.* **54,** 248–251 (2003).
23 Hackman, P., Marchand, S., Sarparanta, J., Vihola, A., Penisson-Besnier, I., Eymard, B. *et al.* Truncating mutations in C-terminal titin may cause more severe tibial muscular dystrophy (TMD). *Neuromuscul. Disord.* **18,** 922–928 (2008).
24 Pollazzon, M., Suominen, T., Penttila, S., Malandrini, A., Carluccio, M. A., Mondelli, M. *et al.* The first Italian family with tibial muscular dystrophy caused by a novel titin mutation. *J. Neurol.* **257,** 575–579 (2010).
25 Udd, B., Rapola, J., Nokelainen, P., Arikawa, E. & Somer, H. Nonvacuolar myopathy in a large family with both late adult onset distal myopathy and severe proximal muscular dystrophy. *J. Neurol. Sci.* **113,** 214–221 (1992).
26 Carmignac, V., Salih, M. A., Quijano-Roy, S., Marchand, S., Al Rayess, M. M., Mukhtar, M. M. *et al.* C-terminal titin deletions cause a novel early-onset myopathy with fatal cardiomyopathy. *Ann. Neurol.* **61,** 340–351 (2007).
27 Labeit, S., Barlow, D. P., Gautel, M., Gibson, T., Holt, J., Hsieh, C. L. *et al.* A regular pattern of two types of 100-residue motif in the sequence of titin. *Nature* **345,** 273–276 (1990).
28 Labeit, S. & Kolmerer, B. Titins: giant proteins in charge of muscle ultrastructure and elasticity. *Science* **270,** 293–296 (1995).
29 Tskhovrebova, L., Walker, M. L., Grossmann, J. G., Khan, G. N., Baron, A. & Trinick, J. Shape and flexibility in the titin 11-domain super-repeat. *J. Mol. Biol.* **397,** 1092–1105 (2010).
30 Bucher, R. M., Svergun, D. I., Muhle-Goll, C. & Mayans, O. The structure of the FnIII Tandem A77-A78 points to a periodically conserved architecture in the myosin-binding region of titin. *J. Mol. Biol.* **401,** 843–853 (2010).
31 Muhle-Goll, C., Habeck, M., Cazorla, O., Nilges, M., Labeit, S. & Granzier, H. Structural and functional studies of titin's fn3 modules reveal conserved surface patterns and binding to myosin S1–a possible role in the Frank-Starling mechanism of the heart. *J. Mol. Biol.* **313,** 431–447 (2001).
32 Bang, M. L., Centner, T., Fornoff, F., Geach, A. J., Gotthardt, M., McNabb, M. *et al.* The complete gene sequence of titin, expression of an unusual approximately 700-kDa titin isoform, and its interaction with obscurin identify a novel Z-line to I-band linking system. *Circ. Res.* **89,** 1065–1072 (2001).
33 Maruyama, K., Yoshioka, T., Higuchi, H., Ohashi, K., Kimura, S. & Natori, R. Connectin filaments link thick filaments and Z lines in frog skeletal muscle as revealed by immunoelectron microscopy. *J. Cell. Biol.* **101,** 2167–2172 (1985).
34 Guo, W., Bharmal, S. J., Esbona, K. & Greaser, M. L. Titin diversity–alternative splicing gone wild. *J. Biomed. Biotechnol.* **2010,** 753675 (2010).

Supplementary Information accompanies the paper on Journal of Human Genetics website (http://www.nature.com/jhg)

CLINICAL REPORT

AMERICAN JOURNAL OF medical genetics PART A

A Transient Myelodysplastic/Myeloproliferative Neoplasm in a Patient With Cardio-Facio-Cutaneous Syndrome and a Germline *BRAF* Mutation

Kazuhito Sekiguchi,[1]* Tomoki Maeda,[1] So-ichi Suenobu,[1,2] Nobutaka Kunisaki,[1] Miki Shimizu,[1] Kyoko Kiyota,[1] Yo-suke Handa,[1] Kensuke Akiyoshi,[1] Seigo Korematsu,[1,3] Yoko Aoki,[4] Yoichi Matsubara,[4] and Tatsuro Izumi[1]

[1]Department of Pediatrics and Child Neurology, Oita University Faculty of Medicine, Oita, Japan

[2]Division of General Pediatrics and Emergency Medicine, Oita University Faculty of Medicine, Oita, Japan

[3]Educational Support for Regional Pediatrics, Oita University Faculty of Medicine, Oita, Japan

[4]Department of Medical Genetics, Tohoku University School of Medicine, Sendai, Japan

Manuscript Received: 4 March 2013; Manuscript Accepted: 26 May 2013

A male infant, born at 32 weeks gestation by cesarean because of hydrops fetalis, presented with multiple anomalies, such as sparse and curly scalp hair, absent eyebrows, frontal bossing, an atrial septal defect, pulmonary artery stenosis, and whole myocardial thickening. He was clinically diagnosed with cardio-facio-cutaneous (CFC) syndrome, and was confirmed to have a germline V-raf murine sarcoma viral oncogene homologue B1 (*BRAF*) c.721 A>C mutation. At 1 month of age, he presented with a transient myelodysplastic/myeloproliferative neoplasm (MDS/MPN), which improved within a month without the administration of antineoplastic agents. This is the first report of CFC syndrome with MDS/MPN. The coexistence of MDS/MPN may be related to this *BRAF* c.721 A>C mutation. © 2013 Wiley Periodicals, Inc.

Key words: cardio-facio-cutaneous syndrome; myelodysplastic/myeloproliferative neoplasm; BRAF; RAS/MAPK syndromes; juvenile myelomonocytic leukemia

How to Cite this Article:
Sekiguchi K, Maeda T, Suenobu S-I, Kunisaki N, Shimizu M, Kiyota K, Handa Y-S, Akiyoshi K, Korematsu S, Aoki Y, Matsubara Y, Izumi T. 2013. A transient myelodysplastic/myeloproliferative neoplasm in a patient with cardio-facio-cutaneous syndrome and a germline BRAF mutation.
Am J Med Genet Part A 161A:2600–2603.

INTRODUCTION

Cardio-facio-cutaneous (CFC) syndrome is genetic disorder characterized by clinical features such as congenital heart defects, a characteristic facial appearance, ectodermal abnormalities and growth failure [Reynolds et al., 1986]. V-raf murine sarcoma viral oncogene homolog B1 (*BRAF*) is one of rat sarcoma viral oncogene homolog/mitogen activated protein kinase (RAS/MAPK) signaling pathway genes, and has been identified as a causative gene of CFC syndrome [reviewed in Aoki et al., 2008 and Denayer and Legius, 2007]. We report on a male infant with CFC syndrome, who was confirmed to have a germline *BRAF* mutation, and then presented with a myelodysplastic/myeloproliferative neoplasm (MDS/MPN) at 1 month of age.

CLINICAL REPORT

A male was born through cesarean at 32 weeks gestation as the first product of healthy nonconsanguineous Japanese parents. His birth weight, length and head circumference were 2,370 g (−0.8 SD), 40.0 cm (+2.3 SD), 34.2 cm (+3.2 SD), respectively. Due to hydrops fetalis and neonatal asphyxia, he required immediate resuscitation. Mechanical ventilation was needed until age 3 months. He presented with multiple anomalies, such as sparse and curly scalp hair, absent eyebrows, frontal bossing with temporal narrowing, ocular hypertelorism, low set ears, a short and webbed neck, and cryptorchidism (Fig. 1). His complete blood counts at age 1 day revealed the following: WBC 12,770/μl (neutrophils 80%,

Conflict of interest: none.

*Correspondence to:
Kazuhito Sekiguchi, Department of Pediatrics and Child Neurology, Oita University Faculty of Medicine, 1-1 Idaigaoka, Hasama, Yufu, Oita 879-5593, Japan.
E-mail: sekiguch@oita-u.ac.jp

Article first published online in Wiley Online Library (wileyonlinelibrary.com): 15 August 2013
DOI 10.1002/ajmg.a.36107

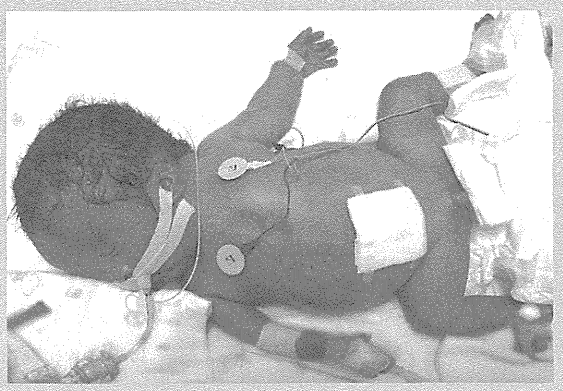

FIG. 1. Full-body image of the patient at birth and his facial features at 3 hours of age. The patient showed severe generalized edema at birth. He presented with sparse and curly hair, frontal bossing, hypertelorism, low-set ears, a short and webbed neck, and cryptorchidism.

lymphocytes 12%, monocytes 6%, myelocytes 2%), RBC 343 × 10^4/μl, erythroblasts 2,430/μl, hemoglobin 14.2g/dl, and platelets 3.2 × 10^4/μl. A chromosome analysis of his peripheral blood lymphocytes showed a 46, XY karyotype. He had an atrial septal defect (ASD), pulmonary artery stenosis (PS), whole myocardial thickening, a pulmonary arteriovenous fistula, an intrahepatic portal systemic shunt, hepatosplenomegaly, right cryptorchidism, a right double renal pelvis, and ureter and agenesis of the corpus callosum. These clinical features were all compatible with CFC syndrome.

At age 1 month, a peripheral blood examination indicated monocytosis of 17% (2,370/μl), with WBC 13,930/μl, RBC 295 × 10^4/μl, and platelets 11.2 × 10^4/μl, with giant platelets. Bone marrow aspiration revealed a nucleated cell count of 9.4 × 10^4/μl, megakaryocyte count 56.2/μl, and did not contain pathologic blasts. The karyotype of the bone marrow cells was 46, XY. The granulocyte-macrophage colony-forming unit (CFU-GM) assay using a semi-solid methylcellulose method showed spontaneous CFU-GM formation of bone marrow (5/5 × 10^4 mononuclear cells) and peripheral blood (35/5 × 10^4 mononuclear cell), without growth factors. Based on these laboratory findings, this patient was diagnosed with MDS/MPN. However, the peripheral blood monocytosis improved without the administration of antineoplastic agents after 1 month with 13% monocytes (1,140/μl), WBC of 8,780/μl, RBC 314 × 10^4/μl, and platelets 26.3 × 10^4/μl. At age 3 years, his complete blood counts revealed 11% monocytes (903/μl), WBC 8,210/μl, RBC 428 × 10^4/μl, and platelets 31.1 × 10^4/μl (Table I). He smiled normally. He demonstrated generalized hypotonia without normal head control and was unable to produce meaningful speech.

CYTOGENETIC AND GENOMIC ANALYSIS

The *BRAF* sequencing analysis showed a heterozygous A>C change at nucleotide 721, resulting in a p.T241P amino acid change in exon 6, which was a previously known mutation in CFC syndrome [Schulz et al., 2008]. No mutations were noted in the Kirsten rat sarcoma viral oncogene homologue (*KRAS*) or protein-tyrosine phosphatase, nonreceptor-type11 (*PTPN11*).

DISCUSSION

A male infant, born via cesarean section because of hydrops fetalis, presented with multiple anomalies suggestive of CFC syndrome. A pulmonary arteriovenous fistula, an intrahepatic portal systemic shunt, hepatosplenomegaly, cryptorchidism, a double renal pelvis, and ureter have been reported as rare complications in CFC syndrome [Narumi et al., 2007]. At 1 month of age, he presented with MDS/MPN, which improved within a month. He showed a germline mutation of *BRAF* c.721 A>C, resulting in a p.T241P amino acid change in exon 6, within a cysteine-rich domain. This mutation was previously described in CFC syndrome [Schulz et al., 2008].

The clinical findings of CFC syndrome are similar to those of other RAS/MAPK or neuro-cardio-facial-cutaneous syndromes, such as Noonan and Costello syndrome [reviewed in Aoki et al., 2008; Denayer and Legius, 2007]. The RAS/MAPK signaling pathway genes, not only *BRAF*, but also *KRAS*, MAPK kinase/ERK kinase 1 (*MEK1*), and MAPK kinase/ERK kinase2 (*MEK2*) have been reported as causative genes for CFC syndrome [Niihori et al., 2006; Rodriguez-Viciana et al., 2006]. CFC syndrome had been considered to have a low risk of malignancy among the various RAS/MAPK syndromes, but a few patients with CFC syndrome due to *BRAF* mutation have presented with malignancies, such as acute lymphoblastic leukemia [van Den Berg and Hennekam, 1999; Makita et al., 2007], and precursor T-lymphoblastic lymphoma [Ohtake et al., 2011].

MDS/MPNs include clonal myeloid neoplasms that at the time of initial presentation have clinical, laboratory or morphologic findings supporting a diagnosis of MDS, and other findings more consistent with MPN. They are usually characterized by hypercellularity of the

TABLE I. Peripheral Blood Examinations of This Patient

Age (months)	0	1	2	12	21	38
WBC (/μl)	12,770	13,930	8,730	8,660	9,040	8,210
Monocytes (/μl)	766	2,370	1,140	866	633	903
RBC (×10^4/μl)	343	295	314	396	404	428
Platelets (×10^4/μl)	3.2	11.2	26.3	24.2	38.6	31.1

bone marrow due to proliferation in one or more of the myeloid lineages [Swerdlow et al., 2008]. Juvenile myelomonocytic leukemia (JMML) is one type of MDS/MPN. Peripheral blood and bone marrow from JMML patients demonstrate spontaneous proliferation according to a CFU-GM assay [Estrov et al., 1986]. Transient monocytosis is not rare in preterm infants [Rajadurai et al., 1992]. Monocytosis in preterm infants is not usually considered a sign of MPD/MPN. In this case, the monocytes proliferation independent of growth factors was noticed according to a CFU-GM assay. The spontaneous proliferation was in favor of MPN. In RAS/MAPK syndromes, occasionally young infants with Noonan syndrome develop a JMML-like disorder which spontaneously resolves without treatment in some, and behaves more aggressively in others [Bader-Meunier et al., 1997; reviewed in Choong et al., 1999]. These children carried germline mutations in *PTPN11* [Tartaglia et al., 2003] or in *KRAS* [Kratz et al., 2005]. *BRAF* mutations had not previously been detected in patients with JMML [de Vries et al., 2007]. This is the first report of a germline *BRAF* mutation and MDS/MPN in a patient with CFC syndrome. The MDS/MPN improved without the administration of antineoplastic agents. This clinical course is similar to the JMML-like disorder observed in Noonan syndrome. This suggests a common mechanism for the development and progression of MDS/MPN in patients with RAS/MAPK syndromes. The MDS/MPN in RAS/MAPK syndrome patients has parallels with the transient leukemia of newborns with Down syndrome. However, the transient leukemia associated with Down syndrome has a high concentration of blasts in the peripheral blood and a GATA binding protein 1 (*GATA1*) mutation as somatic molecular marker [Xu et al., 2003].

The germline *BRAF* mutation site of this patient, c.721 A>C in exon 6, had been reported in two previous patients. One had CFC syndrome [Schulz et al., 2008], and the other had Noonan syndrome with multiple lentigines, previously referred to as LEOPARD syndrome [Sarkozy et al., 2009]. These two patients did not present with malignancies. Garnett and Marais [2004] reviewed the *BRAF* mutations in various adult cancers, and showed that up to 90% of mutations occurred in exon 12. The *BRAF* mutation site of this patient, exon 6, may be related to the spontaneous improvement of his MDS/MPN. A long-term follow-up and additional bone marrow assays might be needed if the patient demonstrates suspicious symptoms with or without peripheral blood monocytosis, because of the risk that MDS/MPN may recur. Further accumulated data about CFC syndrome with a *BRAF* mutation may help to elucidate the basic mechanisms of malignancy, and may suggest a therapeutic strategy.

ACKNOWLEDGMENTS

The authors are grateful to Drs. Hideki Muramatsu and Seiji Kojima, Department of Pediatrics/Developmental Pediatrics, Nagoya University Graduate School of Medicine, Nagoya, for providing important data from the colony assay.

REFERENCES

Aoki Y, Niihori T, Narumi Y, Kure S, Matsubara Y. 2008. The RAS/MAPK syndromes: novel roles of the RAS pathway in human genetic disorders. Hum Mutat 29:992–1006. Review.

Bader-Meunier B, Tchernia G, Miélot F, Fontaine JL, Thomas C, Lyonnet S, Lavergne JM, Dommergues JP. 1997. Occurrence of myelodysplastic/myeloproliferative neoplasm in patients with Noonan syndrome. J Pediatr 130:885–889.

Choong K, Freedman MH, Chitayat D, Kelly EN, Taylor G, Zipursky A. 1999. Juvenile myelomonocytic leukemia and Noonan syndrome. J Pediatr Hematol Oncol 21:523–527. Review.

de Vries AC, Stam RW, Kratz CP, Zenker M, Niemeyer CM, van den Heuvel-Eibrink MM. European Working Group on childhood MDS (EWOG-MDS). 2007. Mutation analysis of the *BRAF* oncogene in juvenile myelomonocytic leukemia. Haematologica 92:1574–1575.

Denayer E, Legius E. 2007. What's new in the neuro-cardio-facial-cutaneous syndromes? Eur J Pediatr 166:1091–1098. Review.

Estrov Z, Grunberger T, Chan HS, Freedman MH. 1986. Juvenile chronic myelogenous leukemia: characterization of the disease using cell cultures. Blood 67:1382–1387.

Garnett MJ, Marais R. 2004. Guilty as charged: *B-RAF* is a human oncogene. Cancer Cell 6:313–319. Review.

Kratz CP, Niemeyer CM, Castleberry RP, Cetin M, Bergsträsser E, Emanuel PD, Hasle H, Kardos G, Klein C, Kojima S, Stary J, Trebo M, Zecca M, Gelb BD, Tartaglia M, Loh ML. 2005. The mutational spectrum of *PTPN11* in juvenile myelomonocytic leukemia and Noonan syndrome/myeloproliferative disease. Blood 106:2183–2185.

Makita Y, Narumi Y, Yoshida M, Niihori T, Kure S, Fujieda K, Matsubara Y, Aoki Y. 2007. Leukemia in Cardio-facio-cutaneous (CFC) syndrome: a patient with a germline mutation in *BRAF* proto-oncogene. J Pediatr Hematol Oncol 29:287–290.

Narumi Y, Aoki Y, Niihori T, Neri G, Cavé H, Verloes A, Nava C, Kavamura MI, Okamoto N, Kurosawa K, Hennekam RC, Wilson LC, Gillessen-Kaesbach G, Wieczorek D, Lapunzina P, Ohashi H, Makita Y, Kondo I, Tsuchiya S, Ito E, Sameshima K, Kato K, Kure S, Matsubara Y. 2007. Molecular and clinical characterization of cardio-facio-cutaneous (CFC) syndrome: Overlapping clinical manifestations with Costello syndrome. Am J Med Genet Part A 143A:799–807.

Niihori T, Aoki Y, Narumi Y, Neri G, Cavé H, Verloes A, Okamoto N, Hennekam RC, Gillessen-Kaesbach G, Wieczorek D, Kavamura MI, Kurosawa K, Ohashi H, Wilson L, Heron D, Bonneau D, Corona G, Kaname T, Naritomi K, Baumann C, Matsumoto N, Kato K, Kure S, Matsubara Y. 2006. Germline *KRAS* and *BRAF* mutations in cardio-facio-cutaneous syndrome. Nat Genet 38:294–296.

Ohtake A, Aoki Y, Saito Y, Niihori T, Shibuya A, Kure S, Matsubara Y. 2011. Non-Hodgkin lymphoma in a patient with cardiofaciocutaneous syndrome. J Pediatr Hematol Oncol 33:e342–e346.

Rajadurai VS, Chambers HM, Vigneswaran R, Gardiner AA. 1992. Monocytosis in preterm infants. Early Hum Dev. 28:223–229.

Reynolds JF, Neri G, Herrmann JP, Blumberg B, Coldwell JG, Miles PV, Opitz JM. 1986. New multiple congenital anomalies/mental retardation syndrome with cardio-facio-cutaneous involvement—The CFC syndrome. Am J Med Genet 25:413–427.

Rodriguez-Viciana P, Tetsu O, Tidyman WE, Estep AL, Conger BA, Cruz MS, McCormick F, Rauen KA. 2006. Germline mutations in genes within the MAPK pathway cause cardio-facio-cutaneous syndrome. Science 311:1287–1290.

Sarkozy A, Carta C, Moretti S, Zampino G, Digilio MC, Pantaleoni F, Scioletti AP, Esposito G, Cordeddu V, Lepri F, Petrangeli V, Dentici ML, Mancini GM, Selicorni A, Rossi C, Mazzanti L, Marino B, Ferrero GB, Silengo MC, Memo L, Stanzial F, Faravelli F, Stuppia L, Puxeddu E, Gelb BD, Dallapiccola B, Tartaglia M. 2009. Germline *BRAF* mutations in Noonan, LEOPARD, and cardiofaciocutaneous syndromes: Molecular diversity and associated phenotypic spectrum. Hum Mutat 30:695–702.

Schulz AL, Albrecht B, Arici C, van der Burgt I, Buske A, Gillessen-Kaesbach G, Heller R, Horn D, Hübner CA, Korenke GC, König R, Kress W, Krüger G, Meinecke P, Mücke J, Plecko B, Rossier E, Schinzel A, Schulze A, Seemanova E, Seidel H, Spranger S, Tuysuz B, Uhrig S, Wieczorek D, Kutsche K, Zenker M. 2008. Mutation and phenotypic spectrum in patients with cardio-facio-cutaneous and Costello syndrome. Clin Genet 73:62–70.

Swerdlow SH, Campo E, Harris NL, Jaffe ES, Pileri SA, Stein H, Thiele J, Vardiman JW. 2008. World Health Organization classification of tumours of haematopoietic and lymphoid tissues. Lyon: International Agency for Research on Cancer.

Tartaglia M, Niemeyer CM, Fragale A, Song X, Buechner J, Jung A, Hählen K, Hasle H, Licht JD, Gelb BD. 2003. Somatic mutations in *PTPN11* in juvenile myelomonocytic leukemia, myelodysplastic syndromes and acute myeloid leukemia. Nat Genet 34:148–150.

van Den Berg H, Hennekam RC. 1999. Acute lymphoblastic leukaemia in a patient with cardiofaciocutaneous syndrome. J Med Genet 36:799–800.

Xu G, Nagano M, Kanezaki R, Toki T, Hayashi Y, Taketani T, Taki T, Mitui T, Koike K, Kato K, Imaizumi M, Sekine I, Ikeda Y, Hanada R, Sako M, Kudo K, Kojima S, Ohneda O, Yamamoto M, Ito E. 2003. Frequent mutations in the *GATA-1* gene in the transient myeloproliferative disorder of Down syndrome. Blood 102:2960–2968.

Hepatology Research

Hepatology Research 2013 doi: 10.1111/hepr.12168

Short Communication

Sequential analysis of amino acid substitutions with hepatitis B virus in association with nucleoside/nucleotide analog treatment detected by deep sequencing

Masashi Ninomiya,[1] Yasuteru Kondo,[1] Tetsuya Niihori,[2] Takeshi Nagashima,[3] Takayuki Kogure,[1] Eiji Kakazu,[1] Osamu Kimura,[1] Yoko Aoki,[2] Yoichi Matsubara[2] and Tooru Shimosegawa[1]

[1]*Division of Gastroenterology, Tohoku University Hospital,* [2]*Department of Medical Genetics, and* [3]*Division of Cell Proliferation, Tohoku University Graduate School of Medicine, Sendai, Japan*

Taking nucleoside/nucleotide analogs is a major antiviral therapy for chronic hepatitis B infection. The problem with this treatment is the selection for drug-resistant mutants. Currently, identification of genotypic drug resistance is conducted by molecular cloning sequenced by the Sanger method. However, this methodology is complicated and time-consuming. These limitations can be overcome by deep sequencing technology. Therefore, we performed sequential analysis of the frequency of drug resistance in one individual, who was treated with lamivudine on-and-off therapy for 2 years, by deep sequencing. The lamivudine-resistant mutations at rtL180M and rtM204V and the entecavir-resistant mutation at rtT184L were detected in the first subject. The lamivudine- and entecavir-resistant strain was still detected in the last subject. However, in the deep sequencing analysis, rt180 of the first subject showed a mixture in 76.9% of the methionine and in 23.1% of the leucine, and rt204 also showed a mixture in 69.0% of the valine and 29.8% of the isoleucine. During the treatment, the ratio of resistant mutations increased. At rt184, the resistant variants were detectable in 58.7% of the sequence, with the replacement of leucine by the wild-type threonine in the first subject. Gradually, entecavir-resistant variants increased in 82.3% of the leucine in the last subject. In conclusion, we demonstrated the amino acid substitutions of the serial nucleoside/nucleotide analog resistants. We revealed that drug-resistant mutants appear unchanged at first glance, but actually there are low-abundant mutations that may develop drug resistance against nucleoside/nucleotide analogs through the selection of dominant mutations.

Key words: amino acid substitutions, deep sequencing, hepatitis B virus, nucleoside/nucleotide analog resistants

Approximately 350–400 million patients are chronically infected with hepatitis B virus (HBV) globally, and the disease has caused epidemics in East Asia.[1,2] In Japan, approximately 1.5 million people are infected with HBV.[3] Chronic hepatitis B (CHB) increases the risk of liver cirrhosis and hepatocellular carcinoma.[4]

Hepatitis B virus is a DNA virus of 3.2 kb surrounded by an envelope of the surface protein (hepatitis B surface antigen [HBsAg]) and it has a circular genome of partially double-stranded DNA.[5] Once the HBV invades into hepatic cells, genomic DNA is transferred to the cell nucleus.[6] In the nucleus, the genomic DNA is converted to a stable intrahepatic reservoir of cccDNA. The cccDNA replicates through an RNA intermediate form by reverse transcription.[7] The purpose of CHB therapy is to achieve sustained suppression of HBV replication and the remission of liver disease. However, cccDNA is resistant to treatment and is not completely eradicated by currently available medications.[8,9] Taking nucleoside/nucleotide analogs (NA) is a major antiviral therapy for the treatment of CHB.[4] Therapies with NA available in Japan include lamivudine (LAM), adefovir dipivoxil (ADV) and entecavir (ETV). They inhibit viral polymerase activity by interfering with the priming of reverse transcription and elongation of the viral minus or plus strand DNA.[10–12] Most patients have chemical and virological responses, but these treatments are hampered by the selection of drug-resistant mutants, leading

Correspondence: Dr Yasuteru Kondo, Division of Gastroenterology, Tohoku University Hospital, 1-1 Seiryo, Aoba-ku, Sendai 980-8574, Japan. Email: yasuteru@ebony.plala.or.jp

The GenBank/EMBL/DDBJ accession numbers for the nucleotide sequences reported in this paper are AB820840-AB820852.

Received 7 March 2013; revision 14 May 2013; accepted 20 May 2013.

to a loss of efficacy, viral relapse and exacerbations of hepatitis after discontinuation.[13]

In the present study, the region of codon rt148 to rt 208 in the polymerase open reading frame was found to include the reported relevant NA-resistant amino acid substitutions. Resistance to LAM has been mapped to the YMDD locus in the C domain of rtM204I/V and is sometimes associated with compensatory mutations in the B domain of rtL180M and/or rtV173L.[14–16] The mutations common to LMV confer cross-resistance and reduced sensitivity to ETV but not to ADV. ETV resistance has been mapped to the B domain with rtI169T, rtL180M and/or rtT184S/A/I/L/F/G/C/M, C domain with rtS202C/G/I and rtM204V/I, and E domain of rtM250I/L/V. The three amino acid substitutions of rtL180 + rtM204 and either rtT184, rtS202 or rtM250 are required for ETV resistance to develop.[17–19] The mutations in the B domain of rtA181S/T/V and D domain of rtN236T were reported to be associated with ADV resistance.[20,21]

Currently, identification of HBV genotypic NA resistance is mainly conducted by polymerase chain reaction (PCR) amplification with Sanger direct sequencing. However, with this method it is difficult to measure the frequencies of each mutation, and it is impossible to detect several mutations combined in the same sequence. It is necessary to find the frequencies of NA-resistant amino acid substitutions, because the secondary compensatory mutations associated with primary NA resistance may restore replication defects or even give rise to multidrug-resistant variants.[19] As an alternative to Sanger direct sequencing, molecular cloning can analyze single viral DNA molecules. However, this methodology is complicated and time-consuming, because analysis of three-digit clones is required to detect variants present in several percent of quasispecies. These limitations can now be overcome by deep sequencing technology.[22] Genetic diversity plays a key role in the NA treatment of HBV infection. Therefore, using this technology, minor HBV variants can be detected, including those with combinations of nucleotide changes in the same period. Detecting low-frequency NA resistants will be important for choosing the NA treatment. In this study, we investigated the transition frequency of amino acid substitutions in NA resistants, in one case using deep sequencing during 2 years of ETV and ADV combination treatment.

A 42-year-old man, diagnosed with CHB infection in June 2005, was treated with LAM on-and-off therapy for 2 years. In HIV-infected patients, on-and-off antiretroviral therapy increased the risk of drug resistance compared with continuous therapy.[23] The HBV DNA levels had gradually increased and ETV treatment was begun in November 2007, but the HBV DNA levels did not decrease, and the treatment was stopped in November 2009. The level of serum transaminase was not elevated at that period. In April 2010, he was seen for the first time in our hospital. The patient was asymptomatic but showed an elevation of transaminase. The following clinical data was indicated: aspartate aminotransferase, 66 IU/L; alanine aminotransferase (ALT), 178 IU/L; positive for HBsAg, hepatitis B e-antigen (HBeAg) and hepatitis B core antibody; HBV genotype C; HBV DNA levels of 1.0×10^8 copies/mL; and negative for anti-hepatitis C virus and anti-HIV. The combination of ETV (0.5 mg/day) and ADV (10 mg/day) therapy was started at that time. After 3 months of therapy, the ALT elevation (119 IU/L) still persisted. Then, the dose of ETV was increased from 0.5 mg to 1.0 mg daily from August 2010. Three months after starting ETV at a dose of 1.0 mg, ALT was at 40 IU/L and HBV DNA had decreased to 6.3×10^3 copies/mL. At the most recent follow up, ALT has remained normal and HBV DNA is at nearly an undetectable level ($<1.3 \times 10^2$ copies/mL). Of note, the serum level of HBeAg is still positive. The changes in viral load and ALT levels are presented in Figure 1(a).

To investigate mutation involved in NA resistance, six serial serum samples of HBV-P10140 (stored in April 2010), HBV-P10193 (June 2010), HBV-P10234 (July 2010), HBV-P10264 (August 2010), HBV-P11021 (January 2011) and 12-009 (January 2012) were enrolled in this study. We extracted HBV DNA by the method described previously with slight modification.[24] Nucleic acids were obtained from 100 μL serum samples using SMITEST EX-R&D (Medical & Biological Laboratories, Nagoya, Japan) and nested PCR was conducted in the presence of PrimeSTAR HS DNA polymerase (TaKaRa Bio, Shiga, Japan) four with primers targeting the polymerase gene of HBV genomes (Table 1). The amplification product of the first-round PCR was 457 bp (nt 596–1052), and that of the second-round PCR was 390 bp (nt 610–999): the nucleotide numbers are in accordance with a genotype B HBV isolate of 3215 nt (accession no. AB010289). The first-round PCR with primers B034 and B037 was conducted for 30 cycles and the second-round PCR for 25 cycles with primers B035 and B036 (Table 1). The second-round PCR amplicons were sequenced directly on both strands using a BigDye Terminator version 3.1 Cycle Sequencing Kit (Applied Biosystems, Foster City, CA, USA) on a 3500xL Genetic Analyzer (Applied Biosystems).

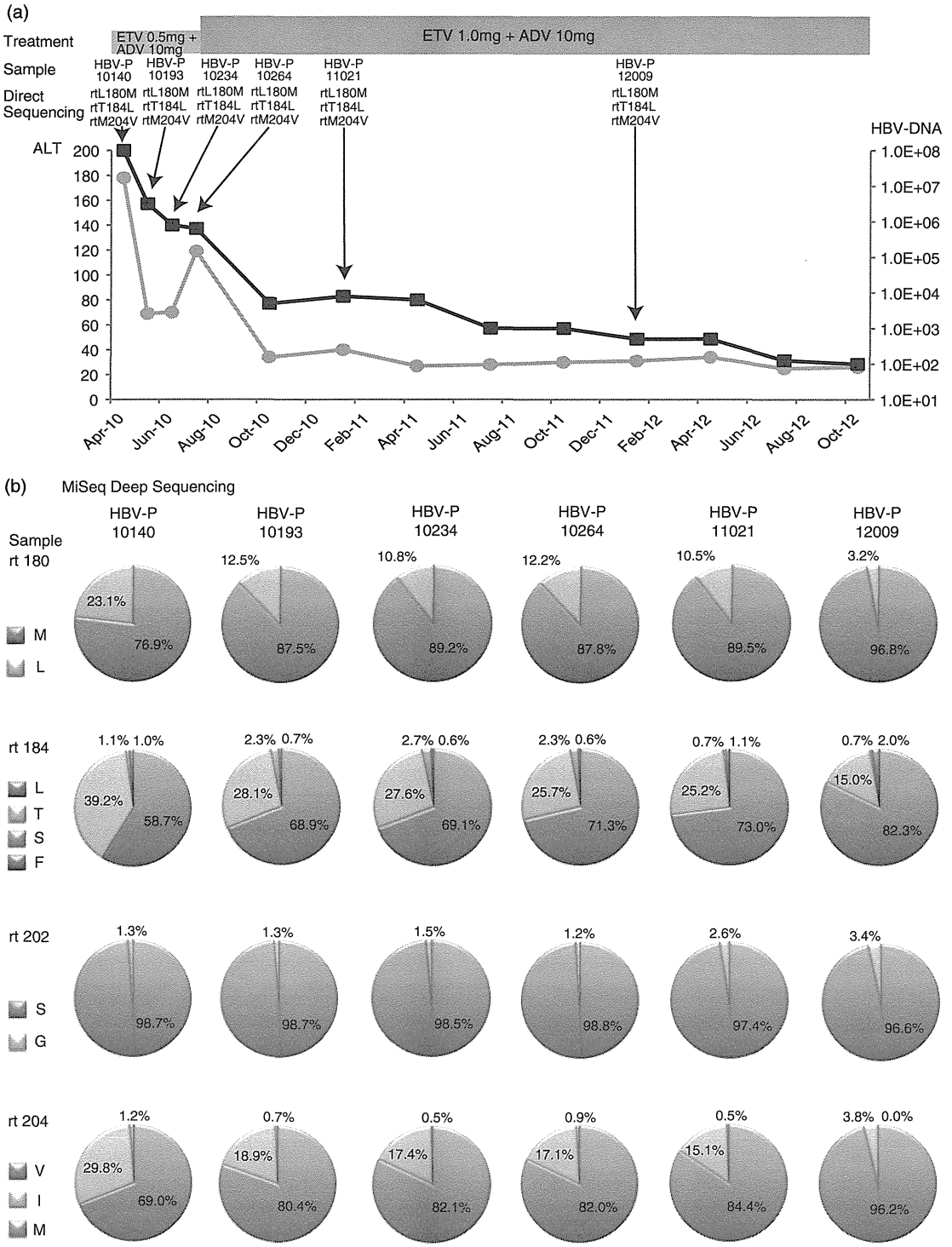

Figure 1 Clinical stage and amino acid substitutions of hepatitis B virus (HBV) resistants. (a) Evolution of HBV DNA viral load, alanine aminotransferase (ALT) levels and resistant HBV variants sequenced directly with Sanger methods in a patient treated sequentially with entecavir (ETV) and adefovir dipivoxil (ADV). (b) Frequency of amino acid substitutions of nucleoside/nucleotide analog (NA)-resistant HBV by MiSeq deep sequencing. M denotes methionine, L denotes leucine, T denotes threonine, V denotes valine, S denotes serine, F denotes phenylalanine, G denotes glycine and I denotes isoleucine. —■—, HBV-DNA; —○—, ALT.

Table 1 Nucleotide sequence of oligonucleotide primers

Primer	Polarity	Usage	Nucleotide sequence
B034	Sense	1st PCR	ACYTGTATTCCCATCCCATC
B037	Antisense	1st PCR	AARGCAGGRTADCCACATTG
B035	Sense	2nd PCR	CCCATCRTCYTGGGCTTTCG
B036	Antisense	2nd PCR	AATTCKYTGACATACTTTCCAATC
P5_B035	Sense	MiSeq sequence	AATGATACGGCGACCACCGAGATCTACACTC TTTCCCTACACGACGCTCTTCCGATCT*CCCA TCRTCYTGGGCTTTCG*
P7_Index1_B036	Antisense	MiSeq sequence of HBV-P10140	CAAGCAGAAGACGGCATACGAGAT***CGTGAT***G TGACTGGAGTTCAGACGTGTGCTCTTCCGA TCT*AATTCKYTGACATACTTTCCAATC*
P7_Index2_B036	Antisense	MiSeq sequence of HBV-P10193	CAAGCAGAAGACGGCATACGAGAT***ACATCG***G TGACTGGAGTTCAGACGTGTGCTCTTCCGAT *CTAATTCKYTGACATACTTTCCAATC*
P7_Index3_B036	Antisense	MiSeq sequence of HBV-P10234	CAAGCAGAAGACGGCATACGAGAT***GCCTAA***GT GACTGGAGTTCAGACGTGTGCTCTTCCGATCT *AATTCKYTGACATACTTTCCAATC*
P7_Index4_B036	Antisense	MiSeq sequence of HBV-P10264	CAAGCAGAAGACGGCATACGAGAT***TGGTCA***GTG ACTGGAGTTCAGACGTGTGCTCTTCCGATCT*AA TTCKYTGACATACTTTCCAATC*
P7_Index5_B036	Antisense	MiSeq sequence of HBV-P11021	CAAGCAGAAGACGGCATACGAGAT***CACTGT***GTG ACTGGAGTTCAGACGTGTGCTCTTCCGATCT*AA TTCKYTGACATACTTTCCAATC*
P7_Index6_B036	Antisense	MiSeq sequence of HBV-P12009	CAAGCAGAAGACGGCATACGAGAT***ATTGGC***GTGA CTGGAGTTCAGACGTGTGCTCTTCCGATCT*AATT CKYTGACATACTTTCCAATC*

Y denotes C or T, R denotes A or G, D denotes A, G or T and K denotes G or T. Italic bold letters indicate the index by multiplex sequencing. Italic letters indicate the nucleotide sequence of B035 or B036.
PCR, polymerase chain reaction.

The LAM-resistant mutations at rtL180M and rtM204V, and the ETV-resistant mutation at rtT184L in HBV-P10140 were detected by direct sequencing. The HBV-mutated LAM- and ETV-resistant strain was still detected in HBV-P12009 and the amino acid substitutions were the same in all subjects (Fig. 1a).

Next, we investigated the frequency of amino acid bases with these same six PCR amplicons by MiSeq (Illumina, San Diego, CA, USA) deep sequencing. MiSeq is the only deep sequencer that quickly integrates amplification, sequencing and data analysis in a single instrument. Compared with HiSeq (Illumina) or Illumina GA IIx, MiSeq can produce longer paired-end reads ($<2 \times 250$) with fewer gigabases of data. However, it has a large enough data volume to sequence PCR amplicons.

A second PCR was performed to attach the required sequencing adaptor for Illumina Miseq sequencing protocol as well as barcode to allow multiplexing of multiple sample libraries per sequencing lane. Six pairs of primers tailed with the adaptor and the specific index were used to amplify six first PCR amplicons. Eight cycles of PCR were performed using PrimeSTAR HS DNA polymerase. All adaptor–barcode–primers are shown in Table 1. The PCR amplicons were purified using AMPure XP beads (Beckman Coulter, Danvers, MA, USA) and the quality and quantity were checked by size range analysis using a D1K ScreenTape on the 2200 Tapestation (Agilent Technologies, Santa Clara, CA, USA). Each library was pooled in equal amounts, and a PhiX control kit (Illumina) was added to 95% of the pooled libraries. Sequencing was performed on MiSeq (Illumina) using 251-bp paired-end reads. Fastq files including demultiplexed sequence reads were generated by Miseq reporter. 251-bp paired-end reads were stripped of low quality 3′-regions using trim galore (www.bioinformatics.babraham.ac.uk/projects/trim_galore/). Sequence reads were aligned with the HBV reference sequence of Yamagata-1 (accession no. AB010289) using of Bowtie 2 (2.1.0).[25] The analysis